Discrete interneuron subsets participate in GluN1/GluN3A excitatory glycine receptor (eGlyR)-mediated regulation of hippocampal network activity throughout development and evolution.

June Hoan Kim[1], Anna Vlachos[1], Vivek Mahadevan[1], Adam P Caccavano[1], Tue Banke[4], Oliver C Crawley[2], Ana I Navarro[2], Xiaoqing Yuan[1], Daniel Abebe[1], Steven Hunt[1], Geoffrey A Vargish[1], Ramesh Chittajallu[1], Mark A G Eldridge[3,8], Reza Azadi[3], Alex C Cummins[3], Anne-Claire Tangen[3], Peyton Harmon[3], Anya Plotnikova[3], Arya Mohanty[3], Elisabetta Furlanis[6,7], Yating Wang[6,7], Min Dai[6,7], Brenda Leyva Garcia[6,7], Ding Liu[4], Zongjian Zhu[4], Hongjie Yuan[4], Samantha L Summer[5], Matthew P Epplin[5], Dennis C Liotta[5], James Pickel[3], Bruno B Averbeck[3], Isabel Perez-Otaño[2], Jordane Dimidschstein[7], Gord Fishell[6,7], Stephen F Traynelis[4], Chris J McBain[1], Kenneth A Pelkey[1]

[1] Section on Cellular and Synaptic Physiology, Eunice Kennedy Shriver National Institute of Child and Human Development, National Institutes of Health, Bethesda, MD 20892, USA
[2] Instituto de Neurociencias (CSIC-UMH), San Juan de Alicante 03550, Spain
[3] Laboratory of Neuropsychology, National Institute of Mental Health (NIMH), NIH, Bethesda, MD, 20892 USA
[4] Department of Pharmacology and Chemical Biology, Emory University School of Medicine, Atlanta, GA, 30322, USA
[5] Department of Chemistry, Emory University, Atlanta, GA, 30322, USA
[6] Department of Neurobiology, Harvard Medical School, Boston, MA, USA
[7] Stanley Center for Psychiatric Research, Broad Institute of Harvard and MIT, Cambridge, MA, USA
[8] Biosciences Institute, Newcastle University, Newcastle upon Tyne NE1 7RU, United Kingdom
Corresponding authors email: pelkeyk2@nih.gov (KAP), mcbainc@nih.gov (CJM)

Summary

Decades of studies implicating GluN3A *N*-methyl-D-aspartate receptor (NMDAR) subunits in physiological and pathological function have largely been interpreted through direct regulation of conventional glutamatergic NMDARs. However, emerging evidence indicates that GluN3A frequently assembles with GluN1 forming unconventional glutamate-insensitive NMDARs that operate as native excitatory glycine receptors (eGlyRs). Here we demonstrate that hippocampal somatostatin and neurogliaform interneurons (Sst-INs and NGFCs) express functional eGlyRs from early postnatal through adult ages. In the developing hippocampus eGlyR-mediated excitation of NGFCs with ambient glycine dramatically increases GABAergic tone, with consequences for the generation of giant depolarizing potentials (GDPs). In the mature hippocampus, eGlyR-mediated excitation of Sst-INs regulates sharp wave ripples (SWRs). Finally, we reveal evolutionary conservation of hippocampal Sst-IN eGlyRs and eGlyR-mediated SWR regulation in non-human primates confirming functional eGlyR availability for therapeutic potential in higher species. Our findings underscore that eGlyR mediated regulation of cell and circuit excitability through both cell autonomous and cell non-autonomous mechanisms must be considered to understand GluN3A roles in brain development, plasticity, and disease.

Introduction

For almost half a century NMDARs have been recognized as crucial mediators of excitatory glutamatergic synapse development, function, and plasticity in brain health and disease. The coincidence detecting features, kinetics, and calcium permeability of conventional GluN1/GluN2 subunit-containing NMDARs confer integrative properties uniquely suited to controlling synaptic maturation, integration, and activity-dependent plasticity [Hansen2021, Nicoll2017]. Interestingly, GluN3A NMDAR subunits are also strongly implicated in nascent synapse and circuit development/plasticity [Das1998, Gonzalez-Gonzalez2023, Hurley2024, Sasaki2002, Tong2008, Roberts2009, Henson2012, Mohamad2013, Kehoe2014, Perez-Otano2016, Crawley2022]. However, emerging evidence indicates that GluN3A subunits primarily co-assemble with GluN1 to yield unconventional glycine (Gly) gated "non-Hebbian NMDARs" that are glutamate insensitive and voltage-independent with low Ca^{2+} permeability [Chatterton2002, Pina-Crespo2010, Awobuluyi2007, Madry2007, Kvist2013a, Bossi2022]. As such GluN1/GluN3 NMDARs are not members of the glutamate receptor family and are referred to as eGlyRs to differentiate them from both conventional glutamate/glycine gated NMDARs and inhibitory chloride conducting pentameric glycine-gated receptors [Chatterton2002, Otsu2019, Crawley2022, Bossi2022, Hurley2024]. Curiously, eGlyRs are often expressed by neurons in forebrain regions essentially devoid of dedicated glycinergic afferents [Zeilhofer2005, Bossi2022, Bossi2023]. Thus, evidence for prototypical rapid, phasic communication through eGlyRs is lacking. Instead, evidence suggests that eGlyRs regulate neuronal excitability by sensing ambient levels of extracellular Gly consistent with observations that surface GluN3A subunits comprise a highly diffusive receptor pool that does not strongly localize to postsynaptic sites [Perez-Otano2006, Otsu2019, Bossi2022, Gonzalez-Gonzalez2023].

Gly gates eGlyRs by binding to GluN3 subunits, whereas Gly binding to GluN1 profoundly desensitizes eGlyRs [Awobuluyi2007, Madry2007, Kvist2013a, Cummings2017, Grand2018, Zhu2020, Rouzbeh2023]. While saturating levels of ambient Gly for GluN1 have historically confounded interrogation of eGlyRs, findings that the glycine site antagonist CGP-78608 (CGP) blocks desensitization and awakens eGlyRs has fostered a new era of cellular and network investigation into this notoriously enigmatic receptor subpopulation that has remained elusive since their discovery in recombinant systems over 20 years ago [Chatterton2002, Matsuda2002, Yao2006, Madry2007, Grand2018, Otsu2019, Zhu2020, Bossi2022, Rouzbeh2023, Hurley2024]. Genetic deletion of *Grin3a*, has revealed critical roles for eGlyRs in regulating diverse behaviors including sensorimotor gating, sleep, place aversion conditioning and fear memory stability [Otsu2019, Bossi2022, Brody2005, Sunagawa2016, Crawley2022]. Moreover, mutations or alterations in *GRIN3A/Grin3a* expression in humans and mice are linked to diverse neurological conditions such as schizophrenia, bipolar disorder, addiction, epilepsy, and Huntington's disease making GluN3A an attractive candidate for therapeutic intervention [Mueller2004, Gallinat2007, Marco2013, Yuan2013, Yang2015, Lee2016, Huang2017, Marco2018, Crawley2022]. The unique features of eGlyR ligand binding, channel activation, and gating can be successfully exploited to develop selective allosteric modulators [Kvist2013a, Kvist2013b, Zhu2020, Rouzbeh2023, Michalski2024, Jacobs2025]. However, determination of therapeutic potential requires thorough characterization of eGlyR function within discrete receptor expressing cell-types across divergent circuits throughout development and across species.

Grin3a expression is particularly high in the developing hippocampus but is not ubiquitous exhibiting unique regional and cell type specific patterns with divergent temporal profiles [Sucher1995, Wong2002, Roberts2009, Kehoe2014, Murillo2021, Hurley2024]. At early postnatal stages *Grin3a* is highly expressed in CA1 pyramidal neurons (PNs) throughout the entire rostrocaudal axis then dramatically declines in dorsal CA1 in adults but remains elevated in ventral CA1 pyramidal neurons [Murillo2021, Hurley2024]. *Grin3a* is not expressed in developing or adult PNs of CA2, CA3, or dentate gyrus indicating that any potential role for *Grin3a* in regulating circuit maturation and function in these hippocampal substructures requires cell non-autonomous mechanisms [Sucher1995, Murillo2021, Beesley2022, Pizzamiglio2025]. Hippocampal and neocortical medial ganglionic eminence (MGE)-derived inhibitory GABAergic interneurons express conspicuously high levels of *Grin3a* throughout development, and adult somatostatin-expressing interneurons (Sst-INs) exhibit robust eGlyR-mediated currents [Pfeffer2013, Paul2017, Murillo2021, Bossi2022, Pizzamiglio2025]. Individual local circuit interneurons widely innervate large numbers of nearby PNs to critically instruct nascent circuit connectivity through early postnatal depolarizing GABAergic drive [Ben-Ari2002, Ben-Ari2007, Cossart2022, Pelkey2017]. Moreover, in mature hippocampus GABAergic inhibition from divergent interneuron subtypes imposes discrete spatiotemporal profiles of inhibition to entrain principal cell assemblies and coordinate network oscillations critical for cognition [Klausberger2008, Stark2014, Pelkey2017, Tzilivaki2023]. These central roles of GABAergic interneurons could be leveraged by ambient Gly through eGlyRs to control network excitability for circuit maturation and rhythmogenesis. Here using a multiparametric approach including transcriptional profiling, conditional loss of function mice, immunohistochemistry, and *ex vivo* electrophysiology with optogenetics and pharmacology we demonstrate that hippocampal Sst-INs and neurogliaform interneurons (NGFCs) express functional eGlyRs from early postnatal through adult ages. Activation of eGlyRs on these interneuron subsets has the capacity to regulate the dominant spontaneous network pacing activities, GDPs and SWRs, in developing and mature hippocampus respectively. Finally, we demonstrate evolutionary conservation of hippocampal Sst-IN eGlyR expression and eGlyR-mediated SWR regulation in the nonhuman primate (NHP) hippocampus confirming functional availability of this target for therapeutic potential in higher mammalian species.

Results

eGlyR modulation of inhibitory drive and network synchronization in the early postnatal hippocampus.

Detailed spatiotemporal profiling using multiplexed fluorescence in situ hybridization (mFISH) revealed remarkably high *Grin3a* expression within MGE-derived hippocampal interneurons, particularly CA1 Sst-INs, at early postnatal ages (~postnatal day (P) 6-9) [Murillo2021]. To initiate our study, we employed Nkx2.1$^{Cre/+}$:Rpl22(RiboTag)$^{HA/HA}$ (MGE-Ribotag) mice to independently validate and extend these findings. This Ribotag-based sequencing strategy provides a robust quantitative platform to examine mRNAs associated with the translational machinery for protein production selectively within the population of MGE-derived interneurons [Mahadevan2020, Sanz2009]. We observed an enrichment of *Grin3a* within hippocampal MGE-derived interneurons relative to bulk hippocampal tissue from early postnatal ages through adulthood (Figure 1A). Notably, bulk hippocampal *Grin3a* levels dramatically declined by 2 months of age, as expected given the well-established reduction in dorsal CA1 PNs [Ciabarra1995, Sucher1995, Sun1998, Sasaki2002, Zhang2002, Perez-Otano2016, Wee2016, Murillo2021, Crawley2022, Bossi2023]. However, MGE-derived interneurons retained high expression of *Grin3a* at all time points examined consistent with findings in adult neocortex [Pfeffer2013, Paul2017, Yao2021, Bossi2022]. Examination of dorsal hippocampal sections from a newly developed mClover-GluN3A reporter mouse line confirmed persistent GluN3A expression in a sparse population of cells outside the PN layer, prominently Sst+ neurons of stratum oriens, at adult stages when CA1 PN labeling is dramatically attenuated (Figure 1B).

At early postnatal ages the hippocampal network is dominated by GABAergic tone that exerts an excitatory influence upon postsynaptic PNs prior to establishment of low intracellular chloride levels by upregulation of KCC2 [Ben-Ari2002, Ben-Ari2007]. Between the ages of P5-10 this depolarizing GABAergic input coordinates spontaneous, synapse-driven network synchronizations in the form of giant depolarizing potentials (GDPs) that propagate throughout the hippocampus to drive activity-dependent circuit maturation and MGE-derived interneurons, particularly Sst-INs, are strongly implicated in this pacing [Ben-Ari1989, Picardo2011, Wester2016, Flossmann2019, Cossart2022]. To probe for eGlyR-mediated regulation of GABAergic tone in the developing hippocampus we recorded spontaneous GABAergic postsynaptic currents (G-PSCs) and the GABAergic component of GDP-associated currents (GDP-Is) in acute hippocampal slices from P5.5–9.5 wild-type and *Grin3a* knockout (*Grin3a*-KO) mice while applying CGP-78608 to remove any eGlyR desensitization (Figure 1C-F). GABAergic synaptic events were electrically isolated by voltage-clamp at 0 mV where both G-PSCs and GDP-Is are detectable as outward $GABA_A$R-mediated currents without significant contamination from phasic glutamatergic transmission (alpha-amino-3-hydroxy-5-methyl-4-isoxazolepropionic acid receptor (AMPAR)-mediated) needed in concert with GABAergic activity to sustain GDPs. Recordings were performed in CA3 PNs which lack *Grin3a* (Figure 1B; Supplemental Figure 1) to limit confounds of pyramidal cell eGlyRs through network effects and conventional NMDARs were blocked to eliminate confounds of CGP-78608 effects at their glycine binding sites. Under these conditions, CGP-78608 robustly increased CA3 PN G-PSC frequencies in WT but not *Grin3a*-KO mice in a reversible fashion (Figure 1C-E). Concomitantly, we consistently observed that GDP-I frequencies

declined by the end of CGP-78608 application in WT mice without consistent effects in *Grin3a*-KOs (Figure 1F). Our initial expression profiling and functional observations suggest that immature hippocampal interneurons express eGlyRs that are liganded and desensitized by ambient Gly levels. Moreover, engaging interneuron eGlyRs has the capacity to dramatically increase their excitability to enhance GABAergic tone throughout the hippocampal circuit and potentially disrupt spontaneous rhythmicity.

Grin3a expression in hippocampal NGFCs and Sst-INs yields functional eGlyRs throughout development that influence excitability.

To obtain a more granular appreciation of *Grin3a* expression within specific interneuron subtypes we analyzed single-cell RNA sequencing (scRNA-seq) data from adult mice when interneuron transcriptional identities are well defined and segregated ([Harris2018, Hodge2019, Krienen2020, Yao2021, Mahadevan2021]). Focusing on GABAergic interneurons from a multi-institute integrated scRNA-seq dataset (see Methods) we confirmed that most Sst-INs express high levels of *Grin3a* consistent with prior studies (Figure 2A;Supplemental Figure 1) [Pfeffer2013, Paul2017, Murillo2021, Bossi2022]. Indeed, *Grin3a* serves as a secondary molecular marker for Sst-INs and within these cells the *Grin3a* locus exhibits prominently open chromatin and low DNA methylation states that are indicative of actively transcribed genes promoting cell identity ([Pfeffer2013, Yao2021]). We also discovered previously unappreciated *Grin3a* expression across most NGFC subsets (Figure 2A; Supplemental Figure 1). Amongst NGFCs *Grin3a* is expressed in both Lamp5^{+}/Lhx6^{+} MGE-derived subsets, also known as Ivy cells (IvyCs), and Lamp5^{+}/Lhx6^{-} caudal ganglionic eminence (CGE)-derived subsets that are both well represented in the rodent hippocampus [Fuentealba2008, Tricoire2010, Tricoire2011]. Consistent with these scRNA-seq profiles mClover-GluN3A labeled cells co-expressed Sst in stratum oriens and neuronal nitric oxide synthase (nNOS) in putative NGFCs that comprise the dominant interneuron subtype in stratum lacunosum moleculare (Figure 2B; Supplemental Figure 1).

To directly confirm functional eGlyR expression within hippocampal interneurons we electrophysiologically measured their responses to brief, pressure applied Gly (10 mM) delivered locally via a glass micropipette (Figure 2C-D). Sst-INs and NGFCs were targeted using Sst-Cre:Ai14 and NPY-Cre:Ai14 tdTomato reporter mice respectively. To pharmacologically isolate eGlyR-mediated currents, we included a cocktail of receptor antagonists in the perfusing artificial cerebrospinal fluid (ACSF) to block conventional ionotropic glycine (strychnine, 1 µM) glutamate (DL-APV, 50 µM, DNQX, 10 µM), and GABA receptors (picrotoxin, 50 µM; bicuculline, 10 µM). With this cocktail any initial current induced by Gly in regular ACSF was essentially abolished indicating minimal eGlyR-mediated current availability (Figure 2C-D and see Supplemental Figure 2 for sequential antagonist example). However, application of CGP-78608 in the presence of the antagonist cocktail unmasked robust Gly-evoked currents in both Sst-INs and NGFCs consistent with mediation through eGlyRs that are desensitized under baseline conditions (Figure 2C-D). Importantly, these Gly-evoked currents required *Grin3a*, as they were absent in either constitutive or conditional *Grin3a* knockout mice (*Grin3a*-KO; Sst-*Grin3a*-cKO and NPY-*Grin3a*-cKO), though ventral CA1 PNs retained CGP-78608 sensitive Gly-evoked currents in both interneuron conditional KOs (Figure 2E). Similarly, recordings from stratum oriens Sst-INs in Nkx2.1-*Grin1*-cKOs lacked CGP-78608 sensitive Gly-evoked currents consistent with the requirement for both

GluN1 and GluN3 to form functional eGlyRs (Figure 2E). Further pharmacological evidence that the currents observed in hippocampal interneurons reflect bona fide eGlyR conductance includes antagonism by the GluN1/3A Gly binding site antagonist 5,7-dichlorokynurenic acid (DCKA) and suppression by the negative allosteric modulator EU1180-438 (Figure 2C-D, [Chatterton2002, Awobuluyi2007, Zhu2020, Bossi2022]). In addition, we found that CGP-78608 unmasked Gly-evoked currents in both Sst-INs and NGFCs displayed significant potentiation in response to a newly developed GluN3-selective positive allosteric modulator of eGlyRs, EU1180-490, identified via focused library screening of human GluN1/GluN3A (Figure 2C-D, [Nguyen2025]). In sum, these findings reveal robust eGlyR expression within hippocampal Sst-INs and NGFCs providing potential cellular mediators for the regulation of GABAergic tone onto CA3 PNs by CGP-78608 in the developing hippocampus. Indeed, a more detailed temporal developmental profiling of pressure applied Gly-evoked responses confirmed functional eGlyR expression within Sst-INs and NGFCs at early postnatal ages with Sst-INs exhibiting a modest reduction in current amplitudes with age and NGFCs displaying increased current amplitudes (Supplemental Figure 3).

Building on these findings, we next investigated whether ambient Gly working through eGlyRs has the capacity to directly modulate excitability of *Grin3a*-expressing hippocampal interneurons as suggested by the ability of CGP-78608 to drive GABAergic tone. First, we assessed whether eGlyRs provide a tonic current in hippocampal interneurons by examining the effects of DCKA on membrane holding/leak currents in the presence of the conventional ionotropic glycinergic, glutamatergic, and GABAergic receptor antagonist cocktail. Application of DCKA modestly reduced inward holding current at -70 mV in NGFCs but not Sst-INs (Figure 3A-B). This differential influence of tonic eGlyR currents in the two hippocampal interneuron subtypes is reminiscent of differences reported between amygdala principal cells and neocortical Sst-INs and may reflect regional and/or cell-type specific differences in ambient *ex vivo* Gly levels, as well as eGlyR redox and desensitization states [Grand2018, Bossi2022]. Although recorded in the same gross *ex vivo* structure under the same recording conditions NGFCs and Sst-INs were targeted in very deep or superficial CA1 respectively potentially with unique microenvironmental influences. Conversely, both NGFCs and Sst-INs consistently displayed an increase in holding current in response to application of CGP-78608 indicating sufficient endogenous ambient Gly levels to ligand and largely desensitize the eGlyRs on both interneuron populations (Figure 3C-D). The effects of CGP-78608 on holding current were reversed by DCKA and enhanced by EU1180-490 consistent with mediation through eGlyRs (Figure 3D and Supplemental Figure 4). Moreover, in the current-clamp recording configuration CGP-78608 depolarized both NGFCs and Sst-INs sufficiently to induce or increase action potential (AP) firing (Figure 3E-F). Interestingly, EU1180-490 alone could also drive increased firing of Sst-INs, suggesting that this positive allosteric modulator may relieve eGlyR desensitization directly (Figure 3F). Together our findings conclusively demonstrate that ambient Gly levels have the capacity to strongly influence NGFC and Sst-IN excitability, and hence circuit GABAergic tone, throughout development via eGlyRs within these interneuron subpopulations.

An unexpectedly outsized contribution from NGFCs/IvyCs in early postnatal GABAergic tone and rhythmicity under control and CGP-78608 conditions.

251 A significant body work has implicated Sst-INs as major contributors to early postnatal
252 hippocampal and neocortical network GABAergic tone, coordination of population synchrony,
253 and circuit connectivity/maturation [Picardo2011, Anastasiades2016, Marques-Smith2016,
254 Oh2016, Tuncdemir2016, Modol2017, Flossmann2019, Wang2019, Su2020, Cossart2022,
255 Dard2022]. However, similar studies regarding the role of NGFCs/IvyCs in nascent network
256 function are lacking despite these cells representing perhaps the most abundant dendrite
257 targeting interneurons of the hippocampus [Bezaire2013, Overstreet-Wadiche2015]. To dissect
258 the contributions of Sst-INs and NGFCs to GABAergic tone and pacing within the developing
259 hippocampus under control and CGP-78608 conditions we employed an optogenetic strategy
260 using conditional expression of the light-activated proton pump Achaerhodopsin-3 (Arch) to
261 silence distinct interneuron populations (Figure 4). First, to determine the maximal effectiveness
262 of this approach we used pan-GABAergic neuron Arch mice generated by driving conditional Arch
263 expression with Cre under control of the vesicular inhibitory amino acid transporter gene (VGAT-
264 Cre:ArCh). In control conditions (normal ACSF) light driven suppression of all GABAergic
265 interneurons immediately and persistently blocked the majority of G-PSCs and GDP-Is recorded
266 in early postnatal CA3 PNs of VGAT-Cre:ArCh mice (Figure 4A, C-F). Any residual G-PSCs and GDP-
267 Is in light could reflect AP independent spontaneous GABA release and/or stochastic escapes from
268 Arch-mediated suppression by interneurons with high input resistance during prolonged light
269 epochs (for example, by a large spontaneous AMPAR-mediated glutamatergic input). The effects
270 of Arch activation on G-PSC and GDP-I frequencies reversed upon light termination which typically
271 yielded a bout of "rebound light-off GDPs" as expected for the synchronous release of
272 interneurons from hyperpolarization that can drive them to AP threshold triggering a window of
273 reverberant network activity due to the excitatory nature of GABA at this stage of development
274 (Figure 4A, G and see [Wester2016, Flossmann2019]). Critically, light driven suppression of
275 interneuron activity in VGAT-Cre:ArCh mice significantly inhibited G-PSCs in the presence of CGP-
276 78608 confirming that our optogenetic approach continues to restrain interneurons under
277 conditions of eGlyR-mediated enhanced excitability (Figure 4B-D).
278 In control conditions, selective silencing of Sst-INs with light while recording from early
279 postnatal CA3 PNs yielded highly inconsistent effects that on average modestly depressed G-PSC
280 frequencies but did not significantly alter GDP-Is (Figure 4A, C-F). Successful light-mediated
281 control of the Sst-IN population was evidenced by the high probability of light-off rebound GDPs
282 observed in Sst-Cre:ArCh mice (Figure 4A, G). Surprisingly, Sst-IN silencing failed to significantly
283 depress G-PSCs in the presence of CGP-78608, suggesting that the massive recruitment of
284 GABAergic tone by eGlyRs occurs largely independent of Sst-IN output (Figure 4B-D). In contrast,
285 optogenetic silencing in NPY-Cre:ArCh mice more closely matched our observations from pan-
286 GABAergic neuron silencing with robust inhibition of G-PSC and GDP-I frequencies in control
287 conditions, generation of rebound light-off GDP-Is, and continued inhibition of G-PSCs in the
288 presence of CGP-78608 (Figure 4). Though NPY is strongly expressed in both NGFCs and Sst-INs,
289 potentially confounding interpretation of our optogenetic results, subtractive reasoning points to
290 an outsized role for NGFCs/IvyCs in providing GABAergic tone and rhythmicity within the early
291 postnatal CA3 hippocampus. Indeed, the inability of selective Sst-IN silencing to match the impact
292 of NPY-IN silencing on control G-PSCs and GDP-Is requires consideration of an NPY^+/Sst^- IN cohort,
293 with NGFCs/IvyCs being the most logical candidates. This interpretation is further bolstered by
294 considering the limited possible sources of GABAergic input recruited by eGlyRs. As NPY-IN, but

not Sst-IN, silencing significantly blocks G-PSCs recruited by eGlyR activation and *Grin3a* expression is largely limited to NGFCs/IvyCs and Sst-INs, our findings implicate NGFCs/IvyCs as the dominant source of CGP-78608 recruited GABAergic tone in the developing CA3 hippocampal circuit.

To independently test whether NGFCs/IvyCs are largely responsible for the increased GABAergic tone recruited by eGlyR activation in early postnatal tissue, we evaluated CGP-78608 effects on G-PSCs and GDP-Is in CA3 PNs of conditional *Grin3a* knockout mice (Figure 5). For these experiments we separated the CGP-78608 effects on G-PSCs and GDP-Is into early and late phases since closer temporal inspection of our recordings in wild type mice revealed that while G-PSC frequencies continually increase and plateau during drug application, GDP-Is undergo biphasic effects first increasing in frequency then decreasing (Figure 5). The initial increase in GDP-I frequency is accompanied by decreasing amplitudes until ultimately events cannot be reliably resolved from the increased G-PSCs (eg. Figure 5A-B). This profile for GDP-Is is consistent with the ability of CGP-78608 to increase IN excitability and ultimately drive them beyond threshold (Figure 3). A transient increase in GDP frequency could reflect enhanced excitability of INs participating in GDP generation and propagation; however, as greater numbers of INs are driven to threshold out of phase with the rhythmic network, and perhaps even into depolarization block, the ability to sustain synchronization may be compromised prompting degradation of GDP-Is into uncoordinated unitary events. Importantly, in constitutive *Grin3a*-KO mice all early and late phase CGP-78608 effects on G-PSCs and GDP-Is are eliminated confirming the pharmacological specificity for *Grin3a*-containing receptors in mediating transient and sustained changes in GABAergic tone and circuit pacing (Figure 5Ca,b,f-Da,b,f). However, selective removal of *Grin3a* across the entire IN population (VGAT-*Grin3a*-cKO mice) eliminated only the CGP-78608 induced increase in G-PSCs and the transient increase in GDP-Is (Figure 5Cc,f-Dc,f). Thus, late-stage GDP inhibition by CGP-78608 could reflect network changes triggered by eGlyRs in PNs, for example through polysynaptic interactions between eGlyR expressing CA1 PNs to the CA3 network that enhance network excitability to disrupt rhythmicity [Sik1994, Kim2015, Bocchio2020]. Surprisingly, but consistent with our optogenetic findings, selective removal of *Grin3a* from Sst-INs had no effect on early or late phase effects of GCP-78608 on CA3 PN G-PSCs or GDP-Is (Figure 5Ce,f-De,f). In contrast, NPY-*Grin3a*-cKO mice failed to exhibit persistent or transient increases in CA3 PN G-PSCs or GDP-Is respectively in response to CGP-78608, essentially phenocopying the VGAT-*Grin3a*-cKO mice (Figure 5Cd,f-Dd,f). These findings are entirely consistent with our optogenetic results further indicating that the majority of GABAergic recruitment onto CA3 PNs by removal of eGlyR desensitization arises from NGFCs/IvyCs highlighting a previously unappreciated critical role for this class of interneuron in nascent hippocampal circuit activity.

eGlyR-mediated excitation of Sst-INs regulates sharp wave ripples in adult hippocampal circuits.

In the mature hippocampus the dominant spontaneous synchronous network signature is that of sharp wave ripples (SWRs) that are typically observed *in vivo* during “off-line” brain states such as quiet wakefulness, consummatory behaviors, and non-REM sleep [Buzsáki2015]. These high-frequency synchronized oscillatory events play a critical role in memory consolidation and cognition by allowing rapid network replay of exploratory driven activity patterns over compressed time periods and are characterized by large-amplitude sharp waves with

339 superimposed high-frequency ripple oscillations [Girardeau2009, Jadhav2012, Buzsáki2015,
340 Joo2018]. SWRs are temporally and spatially coordinated by stereotyped activation and silencing
341 of discrete interneuron subtypes, including Sst-INs with oriens-lacunosum moleculare (OLM) Sst-
342 INs exhibiting suppression or excitation depending on experimental preparation and long-range
343 projecting Sst-INs undergoing strong recruitment during SWRs [Royer2012, Varga2012,
344 Somogyi2014, Buzsáki2015, Katona2017, Szabo2022]. Interestingly, interference with *Grin3a*
345 expression can disrupt cognition and consolidation of episodic memories; however, the influence
346 of eGlyRs on mature hippocampal network oscillations has not been previously investigated
347 [Gallinat2007, Roberts2009, Papenberg2014]. As our findings confirm continued expression of
348 functional eGlyRs in adult hippocampal Sst-INs we directly evaluated whether eGlyRs have the
349 capacity to influence SWR rhythmicity (Figure 6).
350 Spontaneous SWRs were readily detected with local field potential (LFP) recordings in the
351 CA3 PN layer of acute hippocampal slices from adult mice maintained at interface (Figure 6A,
352 [Hajos2009, Pelkey2015]). Importantly, spontaneous SWRs persist, and may even be enhanced,
353 in the absence of conventional NMDAR-mediated transmission, and thus, our recordings were
354 performed with conventional NMDARs blocked to eliminate pharmacological confounds to data
355 interpretation of findings with eGlyR-related compounds [Behrens2005, Colgin2005]. In slices
356 from wild type mice application of CGP-78608 or EU1180-490 significantly depressed the
357 frequency of SWR occurrence in a reversible fashion (Figure 1A-B,E). Inhibition of SWRs by CGP-
358 78608 or EU1180-490 was absent in *Grin3a*-KO mice confirming the pharmacological specificity
359 of these reagents for eGlyRs (Figure 6C,E). Most interestingly, selective removal of *Grin3a* from
360 Sst-INs in Sst-*Grin3*-cKO mice greatly attenuated SWR sensitivity to CGP-78608 compared to
361 control animals leaving modest inhibition that was not significantly different from data obtained
362 in *Grin3a*-KOs (Figure 6D-E). Collectively, these findings illustrate that eGlyRs, particularly those
363 expressed by Sst-INs, have the capacity to influence coordinated network rhythmicity in the adult
364 hippocampus.
365
366 **Evolutionary conservation of eGlyR function in hippocampal interneurons.**
367
368 Genetic mutations or altered expression levels of *GRIN3A* in humans are implicated in cognitive
369 deficits and diverse neurological/neuropsychiatric conditions such as schizophrenia, bipolar
370 disorder, addiction, epilepsy, and Huntington's Disease [Mueller2004, Gallinat2007, Marco2013,
371 Yuan2013, Yang2015, Lee2016, Huang2017, Marco2018, Crawley2022]. Historically,
372 interpretation and posited roles of dysregulated *GRIN3A* in disease progression have focused on
373 potential influences over conventional NMDARs (eg. triheteromeric GluN1/2/3 contributions) and
374 phasic synaptic transmission [Kehoe2013, Perez-Otano2016, Crawley2022]. The emerging
375 picture in mice that GluN3A readily assembles as eGlyRs in diverse neurons expressing *Grin3a* to
376 tonically regulate excitability through ambient Gly provides a new lens through which to consider
377 GluN3A-associated disease etiology [Bossi2023]. However, this demands functional confirmation
378 that eGlyRs are evolutionarily conserved regulators of neuronal excitability. Thus, in our final
379 series of experiments we aimed to validate our rodent findings in higher species by functionally
380 interrogating hippocampal interneurons and network rhythmogenesis in adult non-human
381 primates (NHPs).

Analysis of publicly available scRNA-seq data sets online indicate conserved *GRIN3A* expression within neocortical/hippocampal Sst-INs and NGFCs in both NHPs and humans (Supplemental Figure 5). By mFISH we confirmed that *GRIN3A* exhibits a high degree of colocalization with *SST* and *LAMP5* throughout the adult NHP (rhesus macaque) hippocampus (Figure 7A-B). To facilitate Sst-IN identification for functional evaluation of eGlyRs we intracranially injected adult macaques with novel enhancer based viral tools designed to limit transgene expression to Sst-INs, pAAV-PHP.eB-BiSSTe10-dTomato and pAAV-PHP.eB-BiSSTe4 [Furlanis2025]. Then 5-6 weeks after hippocampal AAV introduction we made acute hippocampal slices and targeted fluorescently labeled cells for electrophysiological interrogation (Figure 7C). Consistent with our mouse findings NHP Sst-INs exhibited CGP-78608 sensitive Gly-evoked excitatory currents in the cocktail of conventional glutamate, GABA, and glycine receptor antagonists (Figure 7D). Importantly, these Gly-evoked currents were facilitated by EU1180-490 consistent with mediation by eGlyRs (Figure 7D). Parallel recordings in NHP anterior hippocampal CA1 PNs similarly yielded CGP-78608 and EU1180-490 sensitive Gly-evoked currents (Figure 7D). Finally, as SWRs are evolutionarily conserved network oscillations observed across multiple species, including NHPs and humans [Buzsáki2015] we assessed whether engaging eGlyRs by removal of desensitization/allosteric enhancement could regulate rhythmicity in NHPs. Congruent with our rodent findings, we found that either CGP-78608 or EU1180-490 significantly depressed the incidence of SWRs recorded in the CA3 PN layer of adult NHP slices in a reversible fashion (Figure 7E). In total our expression and functional profiling confirm strong conservation of eGlyR function over approximately 70-100 million years of evolution validating its relevance as a potential novel therapeutic target to regulate neuronal excitability across a constellation of human neurological and neuropsychiatric disorders.

Discussion

Emerging evidence indicates that GluN3A subunits frequently assemble with GluN1 to form unconventional NMDARs that serve as eGlyRs in diverse neurons throughout the brain, consistent with initial cloning studies [Perez-Otano2001, Chatterton2002, Grand2018, Otsu2019, Zhu2020, Bossi2022, Rouzbeh2023, Pizzamiglio2025]. Our present findings unequivocally demonstrate that *Grin3a*$^{+}$ hippocampal Sst-INs and NGFCs/IvyCs express functional eGlyRs from early postnatal to adult ages and across evolution from mouse to macaque. Excitation of NGFCs/IvyCs and Sst-INs with endogenous ambient glycine through eGlyRs has the capacity to regulate spontaneous synchronized hippocampal network activities throughout development. Putative roles for GluN3A in synapse development and circuit function inferred from preclinical knockout/overexpression studies and genetic mutation linkage clinical studies are often modeled on cell autonomous influences of GluN3A over conventional NMDARs through formation of triheteromeric receptors or by serving as dominant negative subunits. Our findings, combined with others, highlight that eGlyR mediated regulation of cell and circuit excitability through both cell autonomous and cell non-autonomous mechanisms must also be considered to understand the role of *Grin3a*/GluN3A in brain development, plasticity, and disease [Otsu2019, Bossi2022, Hurley2024, Pizzamiglio2025].

The gating of eGlyRs is unusual with glycine serving as both agonist through high affinity GluN3A binding and functional antagonist by driving profound desensitization upon binding the lower affinity GluN1 subunit [Chatterton2002, Yao2006, Awobuluyi2007, Madry2007, Bossi2022]. Thus, eGlyRs are well suited to provide tonic excitation at low levels of ambient glycine with an auto-inactivation mechanism at higher glycine levels to limit receptor mediated hyperexcitability/excitotoxicity. Interestingly, higher ambient glycine levels leading to GluN1 binding will promote a switch to increased phasic glutamatergic excitation by saturating co-agonist GluN1 binding sites of conventional NMDARs concomitant with the suppression of tonic eGlyR mediated excitation. Though we observed a modest influence of tonic eGlyR activation on NGFC resting membrane potential, the robust depolarizing influence of CGP-78608 on both Sst-INs and NGFCs indicates that ambient glycine levels throughout our acute hippocampal slices are by and large sufficient to bind GluN1 subunits and drive eGlyR desensitization. This is consistent with decades of electrophysiological interrogation of conventional NMDARs in acute hippocampal slices across many labs without the need for extracellular glycine supplementation. Our findings mirror observations in amygdala and neocortical Sst-INs that exhibit eGlyR desensitization under basal slice conditions [Bossi2022]. In contrast, under the same conditions eGlyRs in amygdala PNs exhibit minimal desensitization and provide significant tonic depolarizing influence that is titrated through neuromodulation of glycine transporter activity [Bossi2022]. Thus, even within the same gross brain structure under the same conditions eGlyR glycine-binding site occupancies may differ across neuronal subtypes according to differential extracellular ambient glycine levels. A very recent report provided evidence for tonic Gly liganding and depolarizing influence of eGlyRs on interneurons with somatic localization to stratum oriens but not PNs and interneurons residing in CA1 stratum pyramidale [Pizzamiglio2025]. While these findings do not entirely align with our observations, perhaps due to recording conditions and animal ages, they further highlight potential for local Gly microenvironments in modulating cell excitability through eGlyRs. It will be important in future investigations to probe both sources and spatiotemporal plasticity of ambient hippocampal glycine *in vivo* across development. In addition, the physiological conditions and extent to which Sst-IN and NGFC/IvyC eGlyR functions are subject to activity dependent modulation through redox regulation, acidification, and zinc should also be evaluated [Madry2007, Cummings2017]. Moreover, it remains possible that there exists an as yet undiscovered endogenous neuroactive molecule that promotes eGlyR function through removal of desensitization or allosteric potentiation mechanistically analogous to CGP-78608 and 1180-490.

GABAergic INs throughout the neocortex, amygdala, and hippocampus have common developmental origins in the ganglionic eminences and discrete IN subtypes in each of these structures display considerable genetic, physiological, and synaptic connectivity/function homologies [Zeisel2015, Tremblay2016, Pelkey2017, Gouwens2020, Hajos2021, Yao2021]. However, granular investigation can reveal regional differences in receptor expression profiles for homologous IN subpopulations across brain regions [Caccavano2025]. Expression of eGlyRs within Sst-INs is universal across the cortical structures thus far examined ([Bossi2022, Pizzamiglio2025], and present findings). In contrast, parvalbumin (PV) IN expression of eGlyRs appears inconsistent with functional expression demonstrated in amygdala and hippocampal PV INs but not their neocortical counterparts [Bossi2022, Pizzamiglio2025]. Curiously, *Grin3a* is minimally expressed within transcriptionally defined rodent hippocampal and neocortical PV INs,

469 though increases through evolution (Supplemental figure 5). These findings highlight the
470 importance of careful cell-type specific evaluation across brain regions and species in mapping
471 eGlyR expressing neurons to understand their circuit influences and potential for therapeutic
472 leverage. In addition to the utility of emerging nervous system wide transcriptional data sets
473 across species, identification of rodent GluN3A/eGlyR expressing neurons throughout the brain
474 will be greatly facilitated by the newly developed mClover-GluN3A reporter mouse line.
475 Here we further identify hippocampal MGE- and CGE-derived NGFC/IvyC cohorts as neuronal
476 elements through which ambient Gly can regulate circuit function by eGlyR signaling.
477 Transcriptional profiling indicates conserved strong *Grin3a* expression levels in neocortical NGFCs
478 defined by *Id2* and *Lamp5* expression (Supplemental Figure 5A). In evaluating NGFCs/IvyCs
479 through the lens of eGlyRs we discovered a previously unappreciated capacity for these
480 interneurons to dramatically shape GABAergic tone and network pacing in the developing
481 hippocampus. Past studies have largely implicated Sst-INs as major contributors to early
482 postnatal hippocampal and neocortical network GABAergic tone, coordination of population
483 synchrony, and circuit connectivity/maturation [Picardo2011, Anastasiades2016, Marques-
484 Smith2016, Oh2016, Tuncdemir2016, Modol2017, Flossmann2019, Wang2019, Su2020,
485 Cossart2022, Dard2022]. However, while synchronization of Sst-IN activation has the capacity to
486 generate GDP-like events (eg. light off events in Sst-Cre: ArCh) minimizing Sst-IN activity fails to
487 consistently depress spontaneous GABAergic tone or intrinsic GDP pacing in the developing
488 hippocampus (see also [Flossmann2019]). In contrast, the same optogenetic strategy to silence
489 NGFC/IvyC activity consistently suppressed spontaneous GABAergic tone and GDPs in CA3 PNs.
490 Moreover, NGFC/IvyC inputs were found to dominate the excess inhibitory drive recruited by
491 eGlyR activation with CGP-78608 in the immature hippocampus. These findings, together with
492 recent evidence implicating immature parvalbumin interneurons in early network GABAergic
493 pacing [Caccavano2025], highlight the need for further investigation of multiple cardinal IN
494 classes in coordinating developing hippocampal circuit dynamics.
495 The increasing availability of publicly accessible single cell transcriptomic data sets has greatly
496 facilitated genetic profiling of discrete neuronal populations across species as a starting point for
497 validating translational relevance of rodent centric studies to higher species. However,
498 opportunities for functional validation in neuronal cells and circuits of higher species remains
499 limited by tissue availability and genetic identification of discrete cell types. Here we employed
500 recently developed enhancer based AAV tools to facilitate selective targeting of Sst-INs in live NHP
501 tissue for direct functional interrogation of the evolutionary conservation of eGlyR expression in
502 this neuronal subpopulation [Furlanis2025]. Further development of such tools for cell-type
503 specific targeting will greatly expand the discrete neuronal subtypes throughout the brain for
504 targeting across species in preclinical studies requiring selective cell labeling/actuation and for
505 future therapeutic intervention or gene therapy [Tasic2025]. Our findings confirmed that
506 expression of *GRIN3A* is indeed predictive of operational eGlyRs in NHPs as in rodents. The
507 emerging picture from our current findings combined with others [Grand2018, Zhu2020,
508 Bossi2022], necessitate consideration of eGlyR dysregulation in addition to conventional NMDARs
509 as an underlying feature of neurological disorders associated with genetic mutations or
510 alterations in *GRIN3A* expression such as schizophrenia, bipolar disorder, addiction, epilepsy, and
511 Huntington's Disease [Mueller2004, Gallinat2007, Marco2013, Yuan2013, Yang2015, Lee2016,
512 Huang2017, Marco2018, Crawley2022]. Importantly, NHP hippocampal Sst-IN and CA1 PN eGlyRs

513 displayed similar pharmacological profiles to those in rodents with CGP-78608 “awakening” the
514 receptors from desensitization and the newly described allosteric modulator EU1180-490 able to
515 potentiate their responses. Moreover, as in rodents, both compounds worked independent of
516 conventional NMDARs to depress *in vitro* SWR activity, illustrating the ability to leverage eGlyRs
517 expressed in circuit minority cell populations for regulation of network population activities
518 across species. These findings provide a foundation for further native eGlyR evaluation across
519 species in health and disease and confirm their potential as promising therapeutic targets using
520 small molecule selective allosteric modulators.
521
522

Acknowledgements

This research was supported [in part] by the Intramural Research Program of the National Institutes of Health (NIH). The contributions of the NIH author(s) are considered Works of the United States Government. The findings and conclusions presented in this paper are those of the author(s) and do not necessarily reflect the views of the NIH or the U.S. Department of Health and Human Services. We thank Apratim Mitra, Mira Sohn and Ryan Dale (NICHD Bioinformatics and Scientific Programming Core) for assistance with downloading and analyzing scRNAseq datasets. These analyses utilized the computational resources of the NIH Biowulf cluster (http://hpc.nih.gov).

Author contributions

JHK was responsible for project conceptualization, experimental design, electrophysiology experiments, and imaging, analyses. KAP and CJM conceptualized, designed, and supervised the project. JHK, AV GAV, TB, RC, and KAP contributed to electrophysiology experiments. AV and GAV conducted AAV injections and surgery for mice. XY and SH conducted IHC, ISH, morphological reconstructions, and imaging. VM and APV conducted RNAseq analyses, RiboTag experiments and analysis. OCC, AIN and IPO provided Sst-Cre::*Grin3a*$^{fl/fl}$ and mClover-GluN3A reporter IHC analysis. JHK, DA, KP generated Npy-/VGat-Cre:: *Grin3a*$^{fl/fl}$ mice and maintained mouse colonies. DL, ZZ, HY, SFT, SLS, MPE, and DCL provided GluN3a specific allosteric modulators (EU1180-490 and EU1180-438). MAGE, ACC, ACT, PH, AP, AM, JP, and BBA conducted NHP handling, injections, and surgeries. EF, YW, MD, BLG, JD, and GF provided support and design of enhancer AAV constructs. All authors participated in drafting the manuscript with JHK and KAP serving as principal writers. MAGE, BBA, GF, IPO, SFT and CJM provided critical funding support for the study.

Declaration of interests

SFT is a member of the SAB for Eumentis Therapeutics and Neurocrine Biosciences, and a member of the Medical Advisory Board for the GRIN2B Foundation, CureGRIN, and CombinedBrain, co-founder of NeurOp Inc and Agrithera Inc, and a consultant for GRIN Therapeutics and Seyltx. SFT is a PI on a research grant from GRIN Therapeutics to Emory University School of Medicine. SLS, MPE, DCL, and SFT are co-inventors on Emory-owned Intellectual Property that includes allosteric modulators of NMDA receptor function.
The authors declare no further competing interests.

559 **STAR★METHODS**

560 ***KEY RESOURCES TABLE***

REAGENT or RESOURCE	SOURCE	IDENTIFIER
Antibodies		
Rabbit anti-Sst	Thermo Fisher Scientific	Cat# PA5-85759, RRID:AB_ 2792896
Guinea Pig anti-RFP	Synaptic Systems	Cat# 390005, RRID:AB_2737051
Rabbit anti-GFP	Abcam	Cat# ab290, RRID:AB_303395
Rabbit anti-RFP	Antibodies-Online	Cat# ABIN129578, RRID:AB_10781500
AF488 Goat anti-Rabbit IgG (H+L)	Thermo Fisher Scientific	Cat# A-11008, RRID:AB_143165
AF555 Goat anti-Guinea Pig IgG (H+L)	Thermo Fisher Scientific	Cat# A-21435, RRID:AB_2535856
AF488 Goat anti-Rabbit IgG (H+L)	Thermo Fisher Scientific	Cat# A-11034, RRID:AB_2576217
AF555 Goat anti-Rabbit IgG (H+L)	Thermo Fisher Scientific	Cat# A-21429, RRID:AB_2535850
Bacterial and virus strains		
pAAV(AAV5)-pCAG-FLEX-EGFP-WPRE	Addgene[Chen2014]	RRID:Addgene_51502-AAV5
pAAV-PHP.eB-BiSSTe4-dTomato	Addgene [Furlanis2025]	RRID:Addgene_213944
pAAV-PHP.eB-BiSSTe10-dTomato	Addgene [Furlanis2025]	RRID:Addgene_213814
Chemicals, peptides, and recombinant proteins		
DL-APV sodium salt	Abcam	Cat# ab120271
DNQX disodium salt	Abcam	Cat# ab120169
(-)-Bicuculline methobromide	Abcam	Cat# ab120109
Picrotoxin	Abcam	Cat# ab120315
Strychnine	Millipore Sigma	Cat# S0532
CGP-78608 hydrochloride	Tocris	Cat# 1493
EU1180-438	Stephen F Traynelis [Zhu2020]	
EU1180-490	Stephen F Traynelis [Nguyen2025]	
5,7-Dichlorokynurenic Acid, Sodium Salt (DCKA)	Millipore Sigma	Cat# 5.04841
Biocytin	Millipore Sigma	Cat# B4261
AF488 streptavidin	Thermo Fisher Scientific	Cat# S11223
AF555 streptavidin	Thermo Fisher Scientific	Cat# S21381
AF633 streptavidin	Thermo Fisher Scientific	Cat# S21375
DAPI	Millipore Sigma	Cat# D9542
RNAscope Multiplex Fluorescent v2 Assay	Advanced Cell Diagnostic	Cat# 323110
RNAscope mouse probe mmu-Sst	Advanced Cell Diagnostic	Cat# 461681
RNAscope mouse probe mmu-*Grin3a*-C2	Advanced Cell Diagnostic	Cat# 1225361-C2
Opal 520	AKOVA	Cat# OP-001001
Opal 650	AKOVA	Cat# OP-001006
ProLong Gold Antifade Mountant	Thermo Fisher Scientific	Cat# P10144
RNeasy Plus Micro Kit	Qiagen	Cat# 74034
RNA 6000 Pico kit	Agilent	Cat# 5067-1513
SMARTer Stranded Total RNA-Seq. Kit v2	Takara Bio	Cat# 634411

Experimental models: Organisms/strains		
Mouse: B6;129X1-*Grin3a*^{tm1Nnk}/J NR3a KO	The Jackson Laboratory [Das1998]	RRID:IMSR_JAX:029974
Mouse: *Grin3a*$^{fl/fl}$	Isabel Perez-Otano	
Mouse: *Grin1*$^{fl/fl}$	The Jackson Laboratory [Tsien1996]	RRID:IMSR_JAX:005246
Mouse: Sst-Cre::*Grin3a*$^{fl/fl}$	Isabel Perez-Otano Lab	
Mouse: Sst$^{tm2.1(cre)Zjh}$/J Sst-IRES-Cre	The Jackson Laboratory [Taniguchi2011]	RRID:IMSR_JAX:013044
Mouse: B6.Cg-NPY$^{tm1(cre)Zman}$/J NPY-IRES-Cre	The Jackson Laboratory [Milstein2015]	RRID:IMSR_JAX:027851
Mouse: C57BL/6J-Tg(Nkx2-1-cre)2Sand/J Nkx2.1-Cre	The Jackson Laboratory [Xu2008]	RRID:IMSR_JAX:008661
Mouse: Slc32a1$^{tm2(cre)Lowl}$/J VGAT-IRES-Cre	The Jackson Laboratory [Vong2011]	RRID:IMSR_JAX:016962
Mouse: B6.Cg-Gt(ROSA)26Sor$^{tm9(CAG-tdTomato)Hze}$/J Ai9(RCL-tdT)	The Jackson Laboratory [Madisen2010]	RRID:IMSR_JAX:007909
Mouse: B6.Cg-Gt(ROSA)26Sor$^{tm14(CAG-tdTomato)Hze}$/J Ai14(RCL-tdT)-D	The Jackson Laboratory [Madisen2010]	RRID:IMSR_JAX:007914
Mouse: B6.Cg-Gt(ROSA)26Sor$^{tm40.1(CAG-aop3/EGFP)Hze}$/J Ai40(RCL-ArchT/EGFP)-D	The Jackson Laboratory	RRID:IMSR_JAX:021188
Publicly available transcriptomic data, integrated and reanalysed		
scRNAseq data – processed count file and sample metadata (Allen 2019)	[Hodge2019]	https://transcriptomic-viewer-downloads.s3-us-west-2.amazonaws.com/mouse/transcriptome.zip
scRNAseq data – processed count file and sample metadata (Allen 2021)	[Yao2021]	https://assets.nemoarchive.org/dat-jb2f34y
scRNAseq data – processed count file and sample metadata (Harvard 2020)	[Krienen2020]	GSE151761
scRNAseq data – processed count file and sample metadata (Karolinska 2018)	[Harris2018]	GSE99888
scRNAseq data – processed count file and sample metadata (NIH 2021)	[Mahadevan2021]	GSE156201
snRNAseq human data	[Siletti2023]	https://alleninstitute.github.io/abc_atlas_access/descriptions/WHB_dataset.html
snRNAseq and MERFISH mouse data	[Yao2023]	https://alleninstitute.github.io/abc_atlas_access/descriptions/WMB_dataset.html
Software and algorithms		
pClamp 10.6	Molecular Devices	RRID:SCR_011323
Multiclamp 700B	Molecular Devices	RRID:SCR_018455
FIJI (ImageJ)	NIH	RRID:SCR_002285
Excel	Microsoft	RRID:SCR_016137
ZEN Microscopy Software	Zeiss	RRID:SCR_013672
SPOT 5.2	SPOT Imaging	RRID:SCR_014313

MATLAB 2023b	MathWorks	RRID:SCR_001622
R v3.5.0 and greater	R Foundation	https://www.R-project.org
Seurat v3.4	[Stuart2019]	https://github.com/satijalab/seurat
RStudio IDE	RStudio	https://www.rstudio.com
DESeq2	Bioconductor [Love2014]	RRID:SCR_015687

RESOURCE AVAILABILITY

Lead Contact

Further information and requests for resources and reagents should be directed to and will be fulfilled by the lead contact, Kenneth Pelkey (pelkeyk2@nih.gov).

Materials Availability

This study did not generate novel, unique reagents.

Data and Code Availability

Data generated during this study are available upon request.

EXPERIMENTAL MODEL AND STUDY PARTICIPANT DETAILS

Mice

All mice experiments were conducted in accordance with animal protocols approved by animal care and use committee (ACUC) at the National Institute of Child Health and Human Development (ASP# 20-045) and at Emory University.

Targeted neuronal subpopulations were achieved by fluorescently labeling, using Cre-recombinase driven expression of floxed reporters. Experimental offspring were maintained as heterozygous crosses from homozygous Cre-recombinase driver Sst-IRES-Cre (RRID:IMSR_JAX:013044)[Taniguchi2011], NPY-IRES-Cre (RRID:IMSR_JAX:027851)[Milstein2015], Nkx2.1-Cre (RRID:IMSR_JAX:008661)[Xu2008], *Grin1* (RRID:IMSR_JAX:005246) [Tsien1996] mouse lines and homozygous floxed reporters Ai9(RCL-tdT) (RRID:IMSR_JAX:007909)[Madisen2010], Ai14(RCL-tdT)-D (RRID:IMSR_JAX:007914) [Madisen2010], Ai40(RCL-ArchT/EGFP)-D (RRID:IMSR_JAX:021188) lines.

Non-Human Primates (NHPs)

Adult rhesus macaque and marmoset tissue was obtained as described in [Caccavano2025]. All experiments were performed in accordance with the ILAR Guide for the Care and Use of Laboratory Animals and were conducted under Animal Study Protocols approved by the ACUC at the National Institute of Mental Health. All procedures adhered to the applicable Federal and

594 local laws, regulations, and standards, including the Animal Welfare Act and Regulations and
595 Public Health Service policy (PHS2002).
596
597
598 ***METHOD DETAILS***

599 ***Viral Injections (mouse)***

600 For perinatal injections as described in [Caccavano2025], P0 mice were anesthetized by
601 hypothermia. Mice were bilaterally injected free-hand with 1 µL of solution containing
602 pAAV(AAV5)-pCAG-FLEX-EGFP-WPRE (Addgene 51502-AAV5, ≥ 7×10^{12} vg/mL) in the lateral
603 ventricles: 0.8 mm anterior to lambda and 0.8-1 mm lateral to the sagittal suture, using a 32G
604 microliter Neuros Syringe (Hamilton).
605
606
607 ***Viral Injections and brain harvests in NHPs***

608 As described in [Caccavano2025], briefly intracranial macaque injections were targeted using
609 stereotaxic coordinates derived from MRI and delivered using a needle guide for enhanced
610 accuracy [Fredericks2020]. Surgeries were performed under aseptic conditions in a fully
611 equipped operating suite. pAAV-PHP.eB-BiSSTe4-dTomato (Addgene 213944) or pAAV-PHP.eB-
612 BiSSTe10-dTomato (Addgene 213814) (≥ 1×10^{13} vg/mL) was injected into HPC and M1 of 6
613 rhesus macaques. Within HPC, 30-50 µL of total virus was injected, with 15-25 µL of virus
614 injected at each of 2 locations spaced approximately 2 mm apart in the antero-posterior plane,
615 caudal to the level of the uncus. Within M1, 30-40 µL of total virus was injected, with 10 µL of
616 virus injected at each of 3-4 locations spaced approximately 2 mm apart, targeted via direct
617 visualization.
618 For NHP brain extraction, (6-8 weeks after virus injection for macaque), animals were sedated
619 with ketamine/midazolam (ketamine 5-15 mg/kg, midazolam 0.05-0.3 mg/kg) and maintained
620 on isoflurane. A deep level of anesthesia was verified by an absence of toe-pinch and corneal
621 reflex response. Prior to brain removal and blocking, NHPs were transcardially perfused with
622 ice-cold sucrose-substituted artificial cerebrospinal fluid (SSaCSF) containing in mM: 90 Sucrose,
623 80 NaCl, 3.5 KCl, 1.25 NaH_2PO_4, 24 $NaHCO_3$, 10 Glucose, 0.5 CaCl, 4.5 $MgCl_2$ saturated with
624 carbogen (95% O_2, 5% CO_2), with osmolarity 310-320 Osm. Skulls were opened and brain was
625 removed and blocked in cold oxygenated SSACSF then sectioned as described below for mouse
626 tissue.
627

628 ***Acute brain slice preparation***

629 Postnatal (p5–p10) or juvenile (p11–p21) mice were anesthetized with isoflurane and then
630 decapitated. The brain was dissected in ice-cold high-Mg^{2+} low-Na^+ ACSF for postnatal mice,
631 sucrose-substituted ACSF for juvenile or adults. The high-Mg^{2+} low-Na^+ ACSF contains the
632 following (in mM): 130 NaCl, 3.5 KCl, 24 $NaHCO_3$, 1.25 NaH_2PO_4, 4.5 MgCl, 0.5 $CaCl_2$, and 10
633 glucose with osmolarity 300-310 mOsm. The sucrose-substituted ACSF contains in mM 90

634 sucrose, 80 NaCl, 3.5 KCl, 24 $NaHCO_3$, 1.25 NaH_2PO_4, 4.5 MgCl, 0.5 $CaCl_2$, and 10 glucose.
635 Horizontal hippocampal slices (300 μm) were sectioned using a VT-1200S vibratome (Leica
636 Microsystems), then transferred and incubated in high-Mg^{2+} low-Na^+ ACSF at 32°C at least 1
637 hour before recording. Both ACSFs were saturated with 95% O_2 and 5% CO_2.
638
639 ***Ex vivo Electrophysiology recording***

640 The brain slices were transferred to an upright microscope (Zeiss Axioskop 2), perfused at 2-3
641 ml/min with oxygenated ACSF containing in mM 130 NaCl, 3.5 KCl, 24 $NaHCO_3$, 1.25 NaH_2PO_4,
642 1.5 MgCl, 2.5 $CaCl_2$, and 10 glucose, and maintained at a temperature of 32°C-34°C. Electrodes
643 were pulled from borosilicate glass (World Precision Instruments) to a resistance of 2.5–4
644 Mohm using a vertical pipette puller (PP-830, Narishige). Whole-cell patch-clamp recordings
645 were made using a Multiclamp 700B amplifier (Molecular Devices), filtered at 3 kHz (Bessel
646 filter), and digitized at 10-25 kHz (Digidata 1550, Molecular Devices) and pClamp 10.6 software;
647 Molecular Devices). Uncompensated series resistance during recordings ranged from 7 to 30
648 Mohm and was monitored continuously throughout with 5mV voltage steps. In current-clamp
649 mode, cells were hold to -70 mV; in voltage-clamp mode, holding potentials were set to -70 mV
650 for measuring holding current and 0-10 mV for G-PSC and GDP-I. For whole-cell recordings,
651 internal solutions used were as follows. For recording glycine puff response of NGF-INs in
652 [Figure 2C] and action potentials and holding currents in [Figure 3], the internal solution
653 contains the following (in mM): 130 K-gluconate, 5 KCl, 2 $MgCl_2$, 2 MgATP, 0.3 NaGTP, 10 HEPES,
654 0.6 EGTA, and 0.2% biocytin. In other experiments, the internal solution contains in mM 123
655 $CsCH_3SO_4$, 4.5 NaCl, 4 MgATP, 0.4 NaGTP, 10 HEPES, 1 QX-314, 10 Bapta, and 0.2 % biocytin. The
656 pH of internal solutions was adjusted to 7.4, and osmolarity was adjusted to 285-290 mOsm.
657
658 For synaptically isolated conditions, NMDA, AMPA and $GABA_A$ receptors blocked by APV 50 μM,
659 DNQX 10 μM, BIC 10 μM and PTX 50 μM respectively. Binding CGP-78608 to the GluN1 subunit
660 does not only inhibit desensitization of eGlyRs, but also inhibits conventional GluN2-containing
661 NMDAR, influencing (excitatory) post-synaptic current. Thus, for recording network activity
662 changes by CGP-78608 application, the brain slices were incubated in 100 μM APV containing
663 ACSF for at least 1 hour prior to and during recording, to exclude influence of conventional
664 NMDAR-mediated current change by CGP on the GDP generation.
665
666 NGFCs express Neuro peptide Y (NPY) [Price2005, Karagiannis2009, Tricoire2010], and the
667 combination of the NPY-Cre mouse line and the cell location in the stratum lacunosum moleculare
668 (SLM) enables targeted recording of NGFCs. The labeled NPY-NGF-INs showed late spiking, which
669 is the electrophysiological signature of NGF-INs. For targeting Sst-INs, Sst-IRES-Cre::Ai9-tdTomato
670 or Sst-IRES-Cre::Ai14-tdTomato mice were adopted. In some experiments, putative OLM neurons
671 expressing Sst were targeted based on their morphology such as a horizontally oriented cell body
672 shape, and a deep layer location in the SO near the alveus. Their identification was confirmed by
673 extending the axons to reach the SLM through post hoc cell morphology reconstruction using
674 biocytin staining.
675

676 ***Local field potential recording***

677 Local field potential (LFP) recordings were obtained on an interface recording set-up (Scientific
678 System Design Inc.). Brains of adult (>P60) mice were dissected as mentioned above in ice-cold
679 sucrose-substituted ACSF. Horizontal hippocampal slices were sectioned at 350 µm, then
680 transferred to an interface holding chamber with the slices suspended on the surface level of
681 oxygenated 2 mM $MgCl/CaCl_2$ ACSF containing the following (in mM): 130 NaCl, 3.5 KCl, 24
682 $NaHCO_3$, 1.25 NaH_2PO_4, 2 MgCl, 2 $CaCl_2$, and 10 glucose with an osmolarity of 300-310 mOsm.
683 Slices were incubated at 32°C in the holding chamber for 30 minutes, then held at room
684 temperature until recording. Slices were transferred to an upright microscope (Zeiss Stemi 2000-
685 C) and interface chamber, perfused at 2 ml/min with 32°C-34°C oxygenated 2 mM $MgCl/CaCl_2$
686 ACSF containing 50 µM of APV. 3-5 MOhm tip electrodes were filled with 2 mM $MgCl/CaCl_2$
687 ACSF. A Multiclamp 700B amplifier (Molecular Devices) was used to make LFP recordings,
688 filtered at 3 kHz (Bessel filter), and digitized at 10-25 kHz (Axon Digidata 1550, Molecular
689 Devices) to pClamp 10.6 software; Molecular Devices). LFP recordings were conducted in
690 hippocampal CA3 pyramidal cell layer. Spontaneous sharp wave-ripples (SWRs) were recorded in
691 10-minute epochs for baseline, bath-applied drug (1 µM CGP-78608 or 40 µM EU1180-490), and
692 washout conditions. Recording traces were filtered at 1 Hz (high pass). The frequency of SWRs
693 was determined by the number of SWRs detected during a 2-minute period using Clampfit 10
694 software (Molecular Devices). Traces were filtered 150-250 Hz to confirm ripples.
695
696 ***Post hoc morphological Reconstruction***

697 Slices containing biocytin filled cells were fixed in 4 % paraformaldehyde overnight at 4 °C. Then
698 fixed slices were washed in PBS, permeabilized and incubated with Alexa-488, Alexa-555, or
699 Alexa-633 conjugated streptavidin overnight (Molecular Probes). After incubation, slices were
700 washed multiple times and then were resected to 70µm using a freezing microtome (Microm,
701 Whaltham, MA). Slices were mounted on glass slides (Fisherbrand Superfrost Plus, Fisher
702 Scientific) using Mowiol as a mounting medium. Cells were visualized using epifluorescence
703 microscopy (AX70, Olympus). Confocal images of labelled cells were attained on a Zeiss LSM 780
704 microscope (NICHD Imaging and Microscopy Core).
705
706 ***Immunohistochemistry (IHC)***

707 Mice of different ages (P6, 13, and 6 weeks) were deeply anesthetized with isoflurane and
708 transcardially perfused with 4% paraformaldehyde (PFA) in phosphate buffered saline (PBS) pH
709 7.4. Brains were removed, post-fixed 1 hour in the same fixative at 4°C and transferred to 30%
710 sucrose in PBS at 4°C for at least 24 hours before sectioning. 30 µm coronal slices were cut and
711 stored at -20°C in cryoprotectant of PBS, 30% ethylene glycol and 30% glycerol in PBS.
712 Free-floating brain sections were briefly washed in PBS to remove cryoprotectant and then
713 incubated with blocking solution containing 4% normal goat serum (NGS), 1% BSA, 0.1-0.3%
714 Triton X-100 in PBS for 2 hours. Then sections were incubated with primary antibody in 1% NGS,
715 1% BSA, 0.1-0.3% Triton X-100 in PBS overnight at 4ºC. The following primary antibodies were
716 used: rabbit anti-GFP (Synaptic Systems 132002, 1:1000), chicken anti-GFP (Aves labs GFP-1020,
717 1:1000), rabbit anti-SST (Invitrogen PA585759, 1:500), rabbit anti-nNOS (Abcam ab5586, 1:200).

718 Sections were then washed extensively with PBS and incubated with fluorophore conjugated
719 secondary antibody in 1% BSA, 0.1% Triton X-100 in PBS for 2-3 hours at room temperature
720 (overnight at 4°C for dendritic analysis). Secondary antibodies used were: anti-rabbit Alexa 488
721 (Invitrogen A11008 1:750), anti-chicken Alexa 488 (Invitrogen A11039, 1:750) and anti-rabbit
722 Alexa 555 (Invitrogen A21428, 1:500). After PBS washes, sections were counterstained with
723 DAPI, mounted onto Superfrost Plus slides, air-dried, and coverslipped with fluorescence
724 mounting medium.
725
726 ***In situ Hybridization (ISH) RNAscope***

727 To prepare snap frozen tissue for ISH, freshly dissected macaque hippocampal tissues were
728 submerged into 2-methylbutane that was pre-chilled on a dry ice/ethanol bath for 5 minutes.
729 Tissue was removed, wrapped in foil, and stored at -80 °C. 10 µm frozen sections were made
730 using a Leica Cryostat, mounted on Superfrost Plus slides (Fisher Scientific Cat#12-550-15) and
731 stored at -80 °C.
732 Target probes were designed and manufactured by Advanced Cell Diagnostic (ACD): mmu-
733 SST(Cat#461681), mmu-G*rin3a*-C2(Cat#1225361-C2). ISH was performed following the
734 RNAscope Multiplex Fluorescent v2 Assay instructions provided by ACD. Briefly, frozen thin
735 sections were post-fixed in 4% PFA and dehydrated sequentially in 50%, 70% and 100% ethanol.
736 After H2O2 and Protease IV treatment, sections were incubated with probes at 40 °C for 2
737 hours. Probed signals were detected using RNAscope Multiplex Detection v2 kit (ACD, Cat#
738 323110). Opal 520 (AKOYA, Cat# OP-001001) and Opal 650 (AKOYA, Cat# OP-001006) were used
739 to detect C1 (sst) and C2 (*Grin3a*) probes, respectively. After DAPI staining, sections were
740 covered using ProLong Gold Antifade Mountant (ThermoFisher Scientific, Cat# P10144) and
741 cured in darkness before imaging.
742 RNAscope images were acquired on a SLIDEVIEW VS200 slide scanner (Olympus) mounted with
743 an ORCA-Fusion Digital Camera (HAMAMATSU). Hippocampal regions were scanned at 20x and
744 40x for counting and signal colocalization analysis.
745
746 ***RiboTag***

747 This assay was performed as previously described[Sanz2009, Mahadevan2020,
748 Mahadevan2021]. RNA bound with anti-HA immunoprecipitates and RNA from bulk tissue were
749 purified using RNeasy Plus Micro Kit (Qiagen, Cat# 74034) and the quality of RNA was measured
750 using RNA 6000 Pico kit (Agilent, Cat# 5067-1513) and 2100 Bioanalyzer system (Agilent, Cat#
751 G2939BA). cDNA libraries were constructed from 250 pg RNA using the SMARTer Stranded Total
752 RNA-Seq. Kit v2 (Takara Bio, Cat# 634411) from samples with RNA Integrity Numbers > 6.
753 Sequencing of the libraries were performed on the Illumina HiSeq 2500, at 50 million 2 × 100 bp
754 paired-end reads per sample. ~75% of reads were uniquely mapped to genomic features in the
755 reference genome. Bioconductor package DESeq2[Love2014] was used to identify differentially
756 expressed genes (DEG). This package allows for statistical determination of DEGs using a
757 negative binomial distribution model. The resulting values were then adjusted using the
758 Benjamini and Hochberg's method for controlling the false discovery rate.
759

760 ***Quantification and statistical analysis***

761 Data analysis and visualization was conducted by homemade MATLAB codes. GDP-I was
762 detected using simple threshold method after gaussian filtering, and G-PSC detection was
763 achieved by template event detection in Clampfit 10.6. Paired t-test was selected for change of
764 activity by chemical or light stimuli, and Wilcoxon rank sum test was used for comparison
765 between different conditions (*: 0.01 to 0.05, **: 0.001 to 0.01, ***: < 0.001). Summary data
766 are presented as mean ± SEM.
767
768 ***Multi-institute single-cell transcriptome analyses of GABAergic interneurons***

769 Single-nucleus (sn) / single-cell (sc) transcriptomes from mouse cortical and hippocampal
770 regions were downloaded from studies spanning research institutes (Allen Institute:
771 [Hodge2019, Yao2021], Harvard Medical School: [Krienen2020], Karolinska Institute:
772 [Harris2018], NIH: [Mahadevan2021]). HDF5/raw files from these sources were downloaded
773 and converted into Seurat v3-compatible format using custom scripts in R package as described
774 earlier [Chittajallu2020, Ekins2020]. Basic integration, processing and visualization of the scRNA-
775 seq data were performed with the Seurat v3 [Butler2018, Stuart2019] in R environment using R
776 Studio. Briefly, data was preprocessed by removing cells with less than 200 detectable genes
777 and with reads mapping to mitochondrial genes comprising more than 0.05% of total reads.
778 Gene expression counts were then log normalized and the resulting expression matrix was
779 scaled to 10,000 transcripts per cell. Next, the expression values of each gene across all the cells
780 (z-score transformation) were utilized for dimensionality reduction. These were performed
781 using the NormalizeData() and ScaleData() functions in Seurat with default parameters. Next,
782 we identified the top 2000 genes that exhibited high variability across cells and therefore
783 represent unique features of the cell clusters, for downstream analysis using the
784 FindVariableGenes() function, by applying selection.method = "vst" feature. Next, principal
785 component analysis (PCA) was performed, and the top 20 principal components were stored.
786 We clustered the cells using the FindClusters() with a clustering resolution set to 2.0. Using the
787 FindAllMarkers() function at cutoff of genes expressed in 25% of cells, at a logfc.threshold =
788 0.25, we identified the genes that are expressed in each cluster. For each cell type we used the
789 well-established marker genes that uniquely established the cell identity, as previously
790 described in the respective studies. Subsetting only the Gad1 clusters expressing a combination
791 of Lhx6, Pvalb, Sst, Id2 were annotated as MGE-derived GABAergic interneurons, and a
792 combination of Lhx6-negative, Sncg, Vip, Calb2, Meis2, Cnr1, Ntng1, Ndnf were annotated as
793 CGE-derived GABAergic interneurons. The Neurogliaform interneurons that are
794 $Lhx6^+/Lamp5^+/Id2^+$ are annotated as MGE-derived (NGFC.M); and those that are $Lhx6^-$
795 $/Lamp5^+/Id2^+/Ndnf^+$ are annotated as CGE-derived (NGFC.C). In total we used 86,852 GABA-
796 subset sc-transcriptomes in this study. Expression levels of various GABAergic inteneuron
797 positive control genes and expression of *Grin3a* across the GABAergic interneuron clusters are
798 plotted using DotPlot function in Seurat [Figure 2A].
799
800 ***Analyses of publicly available transcriptomic data***

801 For cross-species comparison of *GRIN1* and *GRIN3A* expression, we utilized a publicly available
802 single-nucleus RNA sequencing (snRNA-seq) dataset comparing across neocortical INs in mouse,
803 marmoset, macaque, and human [Krienen2020]. We probed the mean expression across four
804 neocortical IN subpopulations (PV, SST, ID2, VIP) with a gene panel including *GRIN1*, *GRIN3A*,
805 and distinguishing markers *PVALB*, *SST*, *LAMP5*, and *VIP*.
806
807 For further analysis into human single cell expression, we utilized the Allen Institute whole
808 human brain dataset of the single-cell transcriptomes of ~3.4 million cells across the entire
809 human brain [Siletti2023]. To probe our genes and regions of interest, we adapted Python
810 notebooks provided for accessing the Allen Brain Cell (ABC) Atlas
811 (https://alleninstitute.github.io/abc_atlas_access/intro.html). The log2-normalized expression
812 matrices were downloaded and filtered through several criteria to reach the cell types of
813 interest. First, only neurons were considered (~2.5m cells), which were limited to the
814 superclusters “MGE interneuron”, “CGE interneuron”, “LAMP5-LHX6 and Chandelier”,
815 "Hippocampal CA1-3", "Hippocampal CA4", and "Hippocampal dentate gyrus" (~648k cells), and
816 finally to the hippocampal anatomical division (~204k cells). Analysis of PNs was limited to the
817 supercluster level, while INs were further analyzed down to the cluster level to meaningfully
818 group clusters into identifiable interneuron subpopulations (e.g. PV, SST, LAMP5). We calculated
819 the mean log2-normalized expression values across clusters within this subset of cells for a gene
820 panel including: *GAD1*, *GAD2*, *SLC17A7* (VGluT1), *SLC17A6* (VGluT2), *LHX6*, *PROX1*, *PVALB*, *SST*,
821 *VIP*, *LAMP5*, *CCK*, *SNCG*. Using a mean threshold = 2, MGE-PV clusters were defined as those
822 expressing *LHX6*+, *PVALB*+ (MGE_261/263, LLC_264/266, 1480 cells), MGE-SST clusters as
823 *LHX6*+, *SST*+ (MGE_263/239-254/258, LLC_271, 12935 cells), MGE-LAMP5 as *LHX6*+, *LAMP5*+
824 (LLC_266-275, 7663 cells), CGE-LAMP as CGE *LAMP5*+ (CGE_286-288, 6497 cells), CGE-SNCG as
825 CGE *SNCG*+ (CGE_276/277/279/281/285/291, 6604 cells), and CGE-VIP as CGE *VIP*+
826 (CGE_276/280/281/284/285/289-296, 16007 cells). We next downloaded the single-cell gene
827 expression across these defined groups for a gene panel including *GRIN1* and *GRIN3A* to create
828 violin and dot plots via Graphpad Prism. All adapted Python notebooks are available on Github
829 (https://github.com/acaccavano/ABC_Atlas_Kim2025).
830
831 **References**
832
833 Anastasiades, P. G., Marques-Smith, A., Lyngholm, D., Lickiss, T., Raffiq, S., Katzel, D.,
834 Miesenbock, G. and Butt, S. J. (2016) GABAergic interneurons form transient layer-specific
835 circuits in early postnatal neocortex. Nat Commun **7**: 10584.
836 Awobuluyi, M., Yang, J., Ye, Y., Chatterton, J. E., Godzik, A., Lipton, S. A. and Zhang, D. (2007)
837 Subunit-specific roles of glycine-binding domains in activation of NR1/NR3 N-methyl-D-
838 aspartate receptors. Mol Pharmacol **71**(1): 112-122.
839 Beesley, S., Sullenberger, T., Lee, C. and Kumar, S. S. (2022) GluN3 subunit expression correlates
840 with increased vulnerability of hippocampus and entorhinal cortex to neurodegeneration in a
841 model of temporal lobe epilepsy. J Neurophysiol **127**(6): 1496-1510.
842 Behrens, C. J., van den Boom, L. P., de Hoz, L., Friedman, A. and Heinemann, U. (2005) Induction
843 of sharp wave-ripple complexes in vitro and reorganization of hippocampal networks. Nat
844 Neurosci **8**(11): 1560-1567.

845 Ben-Ari, Y., Cherubini, E., Corradetti, R. and Gaiarsa, J. L. (1989) Giant synaptic potentials in
846 immature rat CA3 hippocampal neurones. J Physiol **416**: 303-325.
847 Ben-Ari, Y. (2002) Excitatory actions of gaba during development: the nature of the nurture. Nat
848 Rev Neurosci **3**(9): 728-739.
849 Ben-Ari, Y., Gaiarsa, J. L., Tyzio, R. and Khazipov, R. (2007) GABA: a pioneer transmitter that
850 excites immature neurons and generates primitive oscillations. Physiol Rev **87**(4): 1215-1284.
851 Bezaire, M. J. and Soltesz, I. (2013) Quantitative assessment of CA1 local circuits: knowledge
852 base for interneuron-pyramidal cell connectivity. Hippocampus **23**(9): 751-785.
853 Bocchio, M., Gouny, C., Angulo-Garcia, D., Toulat, T., Tressard, T., Quiroli, E., Baude, A. and
854 Cossart, R. (2020) Hippocampal hub neurons maintain distinct connectivity throughout their
855 lifetime. Nat Commun **11**(1): 4559.
856 Bossi, S., Dhanasobhon, D., Ellis-Davies, G. C. R., Frontera, J., de Brito Van Velze, M., Lourenco, J.,
857 Murillo, A., Lujan, R., Casado, M., Perez-Otano, I., Bacci, A., Popa, D., Paoletti, P. and Rebola, N.
858 (2022) GluN3A excitatory glycine receptors control adult cortical and amygdalar circuits. Neuron
859 **110**(15): 2438-2454 e2438.
860 Bossi, S., Pizzamiglio, L. and Paoletti, P. (2023) Excitatory GluN1/GluN3A glycine receptors
861 (eGlyRs) in brain signaling. Trends Neurosci **46**(8): 667-681.
862 Brody, S. A., Nakanishi, N., Tu, S., Lipton, S. A. and Geyer, M. A. (2005) A developmental
863 influence of the N-methyl-D-aspartate receptor NR3A subunit on prepulse inhibition of startle.
864 Biol Psychiatry **57**(10): 1147-1152.
865 Butler, A., Hoffman, P., Smibert, P., Papalexi, E. and Satija, R. (2018) Integrating single-cell
866 transcriptomic data across different conditions, technologies, and species. Nat Biotechnol **36**(5):
867 411-420.
868 Buzsáki, G. (2015) Hippocampal sharp wave-ripple: A cognitive biomarker for episodic memory
869 and planning. Hippocampus **25**(10): 1073-1188.
870 Caccavano, A. P., Vlachos, A., McLean, N., Kimmel, S., Kim, J. H., Vargish, G., Mahadevan, V.,
871 Hewitt, L., Rossi, A. M., Spineux, I., Wu, S. J., Furlanis, E., Dai, M., Leyva Garcia, B., Wang, Y.,
872 Chittajallu, R., London, E., Yuan, X., Hunt, S., Abebe, D., Eldridge, M. A. G., Cummins, A. C.,
873 Hines, B. E., Plotnikova, A., Mohanty, A., Averbeck, B. B., Zaghloul, K. A., Dimidschstein, J.,
874 Fishell, G., Pelkey, K. A. and McBain, C. J. (2025) Divergent opioid-mediated suppression of
875 inhibition between hippocampus and neocortex across species and development. Neuron
876 **113**(11): 1805-1822 e1807.
877 Chatterton, J. E., Awobuluyi, M., Premkumar, L. S., Takahashi, H., Talantova, M., Shin, Y., Cui, J.,
878 Tu, S., Sevarino, K. A., Nakanishi, N., Tong, G., Lipton, S. A. and Zhang, D. (2002) Excitatory
879 glycine receptors containing the NR3 family of NMDA receptor subunits. Nature **415**(6873): 793-
880 798.
881 Chen, B. C., Legant, W. R., Wang, K., Shao, L., Milkie, D. E., Davidson, M. W., Janetopoulos, C.,
882 Wu, X. F. S., Hammer, J. A., Liu, Z., English, B. P., Mimori-Kiyosue, Y., Romero, D. P., Ritter, A. T.,
883 Lippincott-Schwartz, J., Fritz-Laylin, L., Mullins, R. D., Mitchell, D. M., Bembenek, J. N., Reymann,
884 A. C., Bohme, R., Grill, S. W., Wang, J. T., Seydoux, G., Tulu, U. S., Kiehart, D. P. and Betzig, E.
885 (2014) Lattice light-sheet microscopy: Imaging molecules to embryos at high spatiotemporal
886 resolution. Science **346**(6208): 1257998.

887 Chittajallu, R., Auville, K., Mahadevan, V., Lai, M., Hunt, S., Calvigioni, D., Pelkey, K. A., Zaghloul,
888 K. A. and McBain, C. J. (2020) Activity-dependent tuning of intrinsic excitability in mouse and
889 human neurogliaform cells. Elife **9**.
890 Ciabarra, A. M., Sullivan, J. M., Gahn, L. G., Pecht, G., Heinemann, S. and Sevarino, K. A. (1995)
891 Cloning and characterization of chi-1: a developmentally regulated member of a novel class of
892 the ionotropic glutamate receptor family. J Neurosci **15**(10): 6498-6508.
893 Colgin, L. L., Jia, Y., Sabatier, J. M. and Lynch, G. (2005) Blockade of NMDA receptors enhances
894 spontaneous sharp waves in rat hippocampal slices. Neurosci Lett **385**(1): 46-51.
895 Cossart, R. and Khazipov, R. (2022) How development sculpts hippocampal circuits and function.
896 Physiol Rev **102**(1): 343-378.
897 Cossart, R. and Garel, S. (2022) Step by step: cells with multiple functions in cortical circuit
898 assembly. Nat Rev Neurosci **23**(7): 395-410.
899 Crawley, O., Conde-Dusman, M. J. and Perez-Otano, I. (2022) GluN3A NMDA receptor subunits:
900 more enigmatic than ever? J Physiol **600**(2): 261-276.
901 Cummings, K. A., Belin, S. and Popescu, G. K. (2017) Residues in the GluN1 C-terminal domain
902 control kinetics and pharmacology of GluN1/GluN3A N-methyl-d-aspartate receptors.
903 Neuropharmacology **119**: 40-47.
904 Dard, R. F., Leprince, E., Denis, J., Rao Balappa, S., Suchkov, D., Boyce, R., Lopez, C., Giorgi-Kurz,
905 M., Szwagier, T., Dumont, T., Rouault, H., Minlebaev, M., Baude, A., Cossart, R. and Picardo, M.
906 A. (2022) The rapid developmental rise of somatic inhibition disengages hippocampal dynamics
907 from self-motion. Elife **11**.
908 Das, S., Sasaki, Y. F., Rothe, T., Premkumar, L. S., Takasu, M., Crandall, J. E., Dikkes, P., Conner, D.
909 A., Rayudu, P. V., Cheung, W., Chen, H. S., Lipton, S. A. and Nakanishi, N. (1998) Increased NMDA
910 current and spine density in mice lacking the NMDA receptor subunit NR3A. Nature **393**(6683):
911 377-381.
912 Ekins, T. G., Mahadevan, V., Zhang, Y., D'Amour, J. A., Akgul, G., Petros, T. J. and McBain, C. J.
913 (2020) Emergence of non-canonical parvalbumin-containing interneurons in hippocampus of a
914 murine model of type I lissencephaly. Elife **9**.
915 Flossmann, T., Kaas, T., Rahmati, V., Kiebel, S. J., Witte, O. W., Holthoff, K. and Kirmse, K. (2019)
916 Somatostatin Interneurons Promote Neuronal Synchrony in the Neonatal Hippocampus. Cell
917 Rep **26**(12): 3173-3182 e3175.
918 Fredericks, J. M., Dash, K. E., Jaskot, E. M., Bennett, T. W., Lerchner, W., Dold, G., Ide, D.,
919 Cummins, A. C., Der Minassian, V. H., Turchi, J. N., Richmond, B. J. and Eldridge, M. A. G. (2020)
920 Methods for mechanical delivery of viral vectors into rhesus monkey brain. J Neurosci Methods
921 **339**: 108730.
922 Fuentealba, P., Begum, R., Capogna, M., Jinno, S., Marton, L. F., Csicsvari, J., Thomson, A.,
923 Somogyi, P. and Klausberger, T. (2008) Ivy cells: a population of nitric-oxide-producing, slow-
924 spiking GABAergic neurons and their involvement in hippocampal network activity. Neuron
925 **57**(6): 917-929.
926 Furlanis, E., Dai, M., Leyva Garcia, B., Tran, T., Vergara, J., Pereira, A., Gorissen, B. L., Wills, S.,
927 Vlachos, A., Hairston, A., Dwivedi, D., Du, S., McMahon, J., Huang, S., Morabito, A., Vazquez, A.,
928 Kim, S., Lee, A. T., Chang, E. F., Razzaq, T., Qazi, A., Vargish, G., Yuan, X., Caccavano, A., Hunt, S.,
929 Chittajallu, R., McLean, N., Hewitt, L., Paranzino, E., Rice, H., Cummins, A. C., Plotnikova, A.,
930 Mohanty, A., Tangen, A. C., Shin, J. H., Azadi, R., Eldridge, M. A. G., Alvarez, V. A., Averbeck, B. B.,

931 Alyahyay, M., Vallejo, T. R., Soheib, M., Vattino, L. G., MacGregor, C. P., Chatain, C. P., Banks, E.,
932 Olah, V. J., Naskar, S., Hill, S., Liebergall, S., Badiani, R., Hyde, L., Hanley, E., Xu, Q., Allaway, K. C.,
933 Goldberg, E. M., Rowan, M. J. M., Nowakowski, T. J., Lee, S., Favuzzi, E., Kaeser, P. S., Sjulson, L.,
934 Batista-Brito, R., Takesian, A. E., Ibrahim, L. A., Iqbal, A., Pelkey, K. A., McBain, C. J.,
935 Dimidschstein, J., Fishell, G. and Wang, Y. (2025) An enhancer-AAV toolbox to target and
936 manipulate distinct interneuron subtypes. Neuron **113**(10): 1525-1547 e1515.
937 Gallinat, J., Gotz, T., Kalus, P., Bajbouj, M., Sander, T. and Winterer, G. (2007) Genetic variations
938 of the NR3A subunit of the NMDA receptor modulate prefrontal cerebral activity in humans. J
939 Cogn Neurosci **19**(1): 59-68.
940 Girardeau, G., Benchenane, K., Wiener, S. I., Buzsaki, G. and Zugaro, M. B. (2009) Selective
941 suppression of hippocampal ripples impairs spatial memory. Nat Neurosci **12**(10): 1222-1223.
942 Gonzalez-Gonzalez, I. M., Gray, J. A., Ferreira, J., Conde-Dusman, M. J., Bouchet, D., Perez-Otano,
943 I. and Groc, L. (2023) GluN3A subunit tunes NMDA receptor synaptic trafficking and content
944 during postnatal brain development. Cell Rep **42**(5): 112477.
945 Gouwens, N. W., Sorensen, S. A., Baftizadeh, F., Budzillo, A., Lee, B. R., Jarsky, T., Alfiler, L., Baker,
946 K., Barkan, E., Berry, K., Bertagnolli, D., Bickley, K., Bomben, J., Braun, T., Brouner, K., Casper, T.,
947 Crichton, K., Daigle, T. L., Dalley, R., de Frates, R. A., Dee, N., Desta, T., Lee, S. D., Dotson, N.,
948 Egdorf, T., Ellingwood, L., Enstrom, R., Esposito, L., Farrell, C., Feng, D., Fong, O., Gala, R., Gamlin,
949 C., Gary, A., Glandon, A., Goldy, J., Gorham, M., Graybuck, L., Gu, H., Hadley, K., Hawrylycz, M. J.,
950 Henry, A. M., Hill, D., Hupp, M., Kebede, S., Kim, T. K., Kim, L., Kroll, M., Lee, C., Link, K. E.,
951 Mallory, M., Mann, R., Maxwell, M., McGraw, M., McMillen, D., Mukora, A., Ng, L., Ng, L., Ngo,
952 K., Nicovich, P. R., Oldre, A., Park, D., Peng, H., Penn, O., Pham, T., Pom, A., Popovic, Z.,
953 Potekhina, L., Rajanbabu, R., Ransford, S., Reid, D., Rimorin, C., Robertson, M., Ronellenfitch, K.,
954 Ruiz, A., Sandman, D., Smith, K., Sulc, J., Sunkin, S. M., Szafer, A., Tieu, M., Torkelson, A., Trinh, J.,
955 Tung, H., Wakeman, W., Ward, K., Williams, G., Zhou, Z., Ting, J. T., Arkhipov, A., Sumbul, U.,
956 Lein, E. S., Koch, C., Yao, Z., Tasic, B., Berg, J., Murphy, G. J. and Zeng, H. (2020) Integrated
957 Morphoelectric and Transcriptomic Classification of Cortical GABAergic Cells. Cell **183**(4): 935-
958 953 e919.
959 Grand, T., Abi Gerges, S., David, M., Diana, M. A. and Paoletti, P. (2018) Unmasking
960 GluN1/GluN3A excitatory glycine NMDA receptors. Nat Commun **9**(1): 4769.
961 Hajos, N., Ellender, T. J., Zemankovics, R., Mann, E. O., Exley, R., Cragg, S. J., Freund, T. F. and
962 Paulsen, O. (2009) Maintaining network activity in submerged hippocampal slices: importance
963 of oxygen supply. Eur J Neurosci **29**(2): 319-327.
964 Hajos, N. (2021) Interneuron Types and Their Circuits in the Basolateral Amygdala. Front Neural
965 Circuits **15**: 687257.
966 Hansen, K. B., Wollmuth, L. P., Bowie, D., Furukawa, H., Menniti, F. S., Sobolevsky, A. I., Swanson,
967 G. T., Swanger, S. A., Greger, I. H., Nakagawa, T., McBain, C. J., Jayaraman, V., Low, C. M.,
968 Dell'Acqua, M. L., Diamond, J. S., Camp, C. R., Perszyk, R. E., Yuan, H. and Traynelis, S. F. (2021)
969 Structure, Function, and Pharmacology of Glutamate Receptor Ion Channels. Pharmacol Rev
970 **73**(4): 298-487.
971 Harris, K. D., Hochgerner, H., Skene, N. G., Magno, L., Katona, L., Bengtsson Gonzales, C.,
972 Somogyi, P., Kessaris, N., Linnarsson, S. and Hjerling-Leffler, J. (2018) Classes and continua of
973 hippocampal CA1 inhibitory neurons revealed by single-cell transcriptomics. PLoS Biol **16**(6):
974 e2006387.

975 Henson, M. A., Larsen, R. S., Lawson, S. N., Perez-Otano, I., Nakanishi, N., Lipton, S. A. and
976 Philpot, B. D. (2012) Genetic deletion of NR3A accelerates glutamatergic synapse maturation.
977 PLoS One **7**(8): e42327.
978 Hodge, R. D., Bakken, T. E., Miller, J. A., Smith, K. A., Barkan, E. R., Graybuck, L. T., Close, J. L.,
979 Long, B., Johansen, N., Penn, O., Yao, Z., Eggermont, J., Hollt, T., Levi, B. P., Shehata, S. I.,
980 Aevermann, B., Beller, A., Bertagnolli, D., Brouner, K., Casper, T., Cobbs, C., Dalley, R., Dee, N.,
981 Ding, S. L., Ellenbogen, R. G., Fong, O., Garren, E., Goldy, J., Gwinn, R. P., Hirschstein, D., Keene,
982 C. D., Keshk, M., Ko, A. L., Lathia, K., Mahfouz, A., Maltzer, Z., McGraw, M., Nguyen, T. N., Nyhus,
983 J., Ojemann, J. G., Oldre, A., Parry, S., Reynolds, S., Rimorin, C., Shapovalova, N. V.,
984 Somasundaram, S., Szafer, A., Thomsen, E. R., Tieu, M., Quon, G., Scheuermann, R. H., Yuste, R.,
985 Sunkin, S. M., Lelieveldt, B., Feng, D., Ng, L., Bernard, A., Hawrylycz, M., Phillips, J. W., Tasic, B.,
986 Zeng, H., Jones, A. R., Koch, C. and Lein, E. S. (2019) Conserved cell types with divergent features
987 in human versus mouse cortex. Nature **573**(7772): 61-68.
988 Huang, X., Chen, Y. Y., Shen, Y., Cao, X., Li, A., Liu, Q., Li, Z., Zhang, L. B., Dai, W., Tan, T., Arias-
989 Carrion, O., Xue, Y. X., Su, H. and Yuan, T. F. (2017) Methamphetamine abuse impairs motor
990 cortical plasticity and function. Mol Psychiatry **22**(9): 1274-1281.
991 Hurley, E. P., Mukherjee, B., Fang, L. Z., Barnes, J. R., Barron, J. C., Nafar, F., Hirasawa, M. and
992 Parsons, M. P. (2024) GluN3A and Excitatory Glycine Receptors in the Adult Hippocampus. J
993 Neurosci **44**(42).
994 Jacobs, L., Nguyen, T. T., McCallum, A., Epplin, M. P., Perszyk, R. E., Myers, S. J., Liu, K., Yang, Y.,
995 Westhuyzen, A. E. V. d., Nocilla, K. A., Allen, J., Ullman, E. Z., Liu, D., Du, Y., Yuan, H., Liotta, D. C.
996 and Traynelis, S. F. (2025) A Subunit-Selective Negative Allosteric Modulator of GluN1/GluN3A
997 Glycine-Activated Receptor. Mol Pharmacol(manuscript submitted).
998 Jadhav, S. P., Kemere, C., German, P. W. and Frank, L. M. (2012) Awake hippocampal sharp-wave
999 ripples support spatial memory. Science **336**(6087): 1454-1458.
1000 Joo, H. R. and Frank, L. M. (2018) The hippocampal sharp wave-ripple in memory retrieval for
1001 immediate use and consolidation. Nat Rev Neurosci **19**(12): 744-757.
1002 Karagiannis, A., Gallopin, T., David, C., Battaglia, D., Geoffroy, H., Rossier, J., Hillman, E. M.,
1003 Staiger, J. F. and Cauli, B. (2009) Classification of NPY-expressing neocortical interneurons. J
1004 Neurosci **29**(11): 3642-3659.
1005 Katona, L., Micklem, B., Borhegyi, Z., Swiejkowski, D. A., Valenti, O., Viney, T. J., Kotzadimitriou,
1006 D., Klausberger, T. and Somogyi, P. (2017) Behavior-dependent activity patterns of GABAergic
1007 long-range projecting neurons in the rat hippocampus. Hippocampus **27**(4): 359-377.
1008 Kehoe, L. A., Bernardinelli, Y. and Muller, D. (2013) GluN3A: an NMDA receptor subunit with
1009 exquisite properties and functions. Neural Plast **2013**: 145387.
1010 Kehoe, L. A., Bellone, C., De Roo, M., Zandueta, A., Dey, P. N., Perez-Otano, I. and Muller, D.
1011 (2014) GluN3A promotes dendritic spine pruning and destabilization during postnatal
1012 development. J Neurosci **34**(28): 9213-9221.
1013 Kim, J. H., Lee, H. J., Min, C. H. and Lee, K. J. (2015) Coherence resonance in bursting neural
1014 networks. Phys. Rev. E **92**(4): 042701.
1015 Klausberger, T. and Somogyi, P. (2008) Neuronal diversity and temporal dynamics: the unity of
1016 hippocampal circuit operations. Science **321**(5885): 53-57.
1017 Krienen, F. M., Goldman, M., Zhang, Q., R, C. H. D. R., Florio, M., Machold, R., Saunders, A.,
1018 Levandowski, K., Zaniewski, H., Schuman, B., Wu, C., Lutservitz, A., Mullally, C. D., Reed, N., Bien,

1019 E., Bortolin, L., Fernandez-Otero, M., Lin, J. D., Wysoker, A., Nemesh, J., Kulp, D., Burns, M.,
1020 Tkachev, V., Smith, R., Walsh, C. A., Dimidschstein, J., Rudy, B., L, S. K., Berretta, S., Fishell, G.,
1021 Feng, G. and McCarroll, S. A. (2020) Innovations present in the primate interneuron repertoire.
1022 Nature **586**(7828): 262-269.
1023 Kvist, T., Greenwood, J. R., Hansen, K. B., Traynelis, S. F. and Brauner-Osborne, H. (2013a)
1024 Structure-based discovery of antagonists for GluN3-containing N-methyl-D-aspartate receptors.
1025 Neuropharmacology **75**: 324-336.
1026 Kvist, T., Steffensen, T. B., Greenwood, J. R., Mehrzad Tabrizi, F., Hansen, K. B., Gajhede, M.,
1027 Pickering, D. S., Traynelis, S. F., Kastrup, J. S. and Brauner-Osborne, H. (2013b) Crystal structure
1028 and pharmacological characterization of a novel N-methyl-D-aspartate (NMDA) receptor
1029 antagonist at the GluN1 glycine binding site. J Biol Chem **288**(46): 33124-33135.
1030 Lee, J. H., Wei, L., Deveau, T. C., Gu, X. and Yu, S. P. (2016) Expression of the NMDA receptor
1031 subunit GluN3A (NR3A) in the olfactory system and its regulatory role on olfaction in the adult
1032 mouse. Brain Struct Funct **221**(6): 3259-3273.
1033 Love, M. I., Huber, W. and Anders, S. (2014) Moderated estimation of fold change and dispersion
1034 for RNA-seq data with DESeq2. Genome Biol **15**(12): 550.
1035 Madisen, L., Zwingman, T. A., Sunkin, S. M., Oh, S. W., Zariwala, H. A., Gu, H., Ng, L. L., Palmiter,
1036 R. D., Hawrylycz, M. J., Jones, A. R., Lein, E. S. and Zeng, H. (2010) A robust and high-throughput
1037 Cre reporting and characterization system for the whole mouse brain. Nat Neurosci **13**(1): 133-
1038 140.
1039 Madry, C., Mesic, I., Bartholomaus, I., Nicke, A., Betz, H. and Laube, B. (2007) Principal role of
1040 NR3 subunits in NR1/NR3 excitatory glycine receptor function. Biochem Biophys Res Commun
1041 **354**(1): 102-108.
1042 Mahadevan, V., Peltekian, A. and McBain, C. J. (2020) Translatome Analyses Using Conditional
1043 Ribosomal Tagging in GABAergic Interneurons and Other Sparse Cell Types. Curr Protoc Neurosci
1044 **92**(1): e93.
1045 Mahadevan, V., Mitra, A., Zhang, Y., Yuan, X., Peltekian, A., Chittajallu, R., Esnault, C., Maric, D.,
1046 Rhodes, C., Pelkey, K. A., Dale, R., Petros, T. J. and McBain, C. J. (2021) NMDARs Drive the
1047 Expression of Neuropsychiatric Disorder Risk Genes Within GABAergic Interneuron Subtypes in
1048 the Juvenile Brain. Front Mol Neurosci **14**: 712609.
1049 Marco, S., Giralt, A., Petrovic, M. M., Pouladi, M. A., Martinez-Turrillas, R., Martinez-Hernandez,
1050 J., Kaltenbach, L. S., Torres-Peraza, J., Graham, R. K., Watanabe, M., Lujan, R., Nakanishi, N.,
1051 Lipton, S. A., Lo, D. C., Hayden, M. R., Alberch, J., Wesseling, J. F. and Perez-Otano, I. (2013)
1052 Suppressing aberrant GluN3A expression rescues synaptic and behavioral impairments in
1053 Huntington's disease models. Nat Med **19**(8): 1030-1038.
1054 Marco, S., Murillo, A. and Perez-Otano, I. (2018) RNAi-Based GluN3A Silencing Prevents and
1055 Reverses Disease Phenotypes Induced by Mutant huntingtin. Mol Ther **26**(8): 1965-1972.
1056 Marques-Smith, A., Lyngholm, D., Kaufmann, A. K., Stacey, J. A., Hoerder-Suabedissen, A.,
1057 Becker, E. B., Wilson, M. C., Molnar, Z. and Butt, S. J. (2016) A Transient Translaminar GABAergic
1058 Interneuron Circuit Connects Thalamocortical Recipient Layers in Neonatal Somatosensory
1059 Cortex. Neuron **89**(3): 536-549.
1060 Matsuda, K., Kamiya, Y., Matsuda, S. and Yuzaki, M. (2002) Cloning and characterization of a
1061 novel NMDA receptor subunit NR3B: a dominant subunit that reduces calcium permeability.
1062 Brain Res Mol Brain Res **100**(1-2): 43-52.

1063 Michalski, K. and Furukawa, H. (2024) Structure and function of GluN1-3A NMDA receptor
1064 excitatory glycine receptor channel. Sci Adv **10**(15): eadl5952.
1065 Milstein, A. D., Bloss, E. B., Apostolides, P. F., Vaidya, S. P., Dilly, G. A., Zemelman, B. V. and
1066 Magee, J. C. (2015) Inhibitory Gating of Input Comparison in the CA1 Microcircuit. Neuron **87**(6):
1067 1274-1289.
1068 Modol, L., Sousa, V. H., Malvache, A., Tressard, T., Baude, A. and Cossart, R. (2017) Spatial
1069 Embryonic Origin Delineates GABAergic Hub Neurons Driving Network Dynamics in the
1070 Developing Entorhinal Cortex. Cereb Cortex **27**(9): 4649-4661.
1071 Mohamad, O., Song, M., Wei, L. and Yu, S. P. (2013) Regulatory roles of the NMDA receptor
1072 GluN3A subunit in locomotion, pain perception and cognitive functions in adult mice. J Physiol
1073 **591**(1): 149-168.
1074 Mueller, H. T. and Meador-Woodruff, J. H. (2004) NR3A NMDA receptor subunit mRNA
1075 expression in schizophrenia, depression and bipolar disorder. Schizophr Res **71**(2-3): 361-370.
1076 Murillo, A., Navarro, A. I., Puelles, E., Zhang, Y., Petros, T. J. and Perez-Otano, I. (2021) Temporal
1077 Dynamics and Neuronal Specificity of Grin3a Expression in the Mouse Forebrain. Cereb Cortex
1078 **31**(4): 1914-1926.
1079 Nguyen, T. T., Zhu, Z., Epplin, M. P., Summer, S. L., Kelsey A, N., Mohan, A., Yuan, H., Hansen, K.
1080 B., Liotta, D. C. and Traynelis, S. F. (2025) Selective Positive Allosteric Modulators of
1081 GluN1/GluN3A Receptors. (Manuscript in preparation).
1082 Nicoll, R. A. (2017) A Brief History of Long-Term Potentiation. Neuron **93**(2): 281-290.
1083 Oh, W. C., Lutzu, S., Castillo, P. E. and Kwon, H. B. (2016) De novo synaptogenesis induced by
1084 GABA in the developing mouse cortex. Science **353**(6303): 1037-1040.
1085 Otsu, Y., Darcq, E., Pietrajtis, K., Matyas, F., Schwartz, E., Bessaih, T., Abi Gerges, S., Rousseau, C.
1086 V., Grand, T., Dieudonne, S., Paoletti, P., Acsady, L., Agulhon, C., Kieffer, B. L. and Diana, M. A.
1087 (2019) Control of aversion by glycine-gated GluN1/GluN3A NMDA receptors in the adult medial
1088 habenula. Science **366**(6462): 250-254.
1089 Overstreet-Wadiche, L. and McBain, C. J. (2015) Neurogliaform cells in cortical circuits. Nat Rev
1090 Neurosci **16**(8): 458-468.
1091 Papenberg, G., Li, S. C., Nagel, I. E., Nietfeld, W., Schjeide, B. M., Schroder, J., Bertram, L.,
1092 Heekeren, H. R., Lindenberger, U. and Backman, L. (2014) Dopamine and glutamate receptor
1093 genes interactively influence episodic memory in old age. Neurobiol Aging **35**(5): 1213 e1213-
1094 1218.
1095 Paul, A., Crow, M., Raudales, R., He, M., Gillis, J. and Huang, Z. J. (2017) Transcriptional
1096 Architecture of Synaptic Communication Delineates GABAergic Neuron Identity. Cell **171**(3):
1097 522-539 e520.
1098 Pelkey, K. A., Barksdale, E., Craig, M. T., Yuan, X., Sukumaran, M., Vargish, G. A., Mitchell, R. M.,
1099 Wyeth, M. S., Petralia, R. S., Chittajallu, R., Karlsson, R. M., Cameron, H. A., Murata, Y.,
1100 Colonnese, M. T., Worley, P. F. and McBain, C. J. (2015) Pentraxins coordinate excitatory synapse
1101 maturation and circuit integration of parvalbumin interneurons. Neuron **85**(6): 1257-1272.
1102 Pelkey, K. A., Chittajallu, R., Craig, M. T., Tricoire, L., Wester, J. C. and McBain, C. J. (2017)
1103 Hippocampal GABAergic Inhibitory Interneurons. Physiol Rev **97**(4): 1619-1747.
1104 Perez-Otano, I., Schulteis, C. T., Contractor, A., Lipton, S. A., Trimmer, J. S., Sucher, N. J. and
1105 Heinemann, S. F. (2001) Assembly with the NR1 subunit is required for surface expression of
1106 NR3A-containing NMDA receptors. J Neurosci **21**(4): 1228-1237.

1107 Perez-Otano, I., Lujan, R., Tavalin, S. J., Plomann, M., Modregger, J., Liu, X. B., Jones, E. G.,
1108 Heinemann, S. F., Lo, D. C. and Ehlers, M. D. (2006) Endocytosis and synaptic removal of NR3A-
1109 containing NMDA receptors by PACSIN1/syndapin1. Nat Neurosci **9**(5): 611-621.
1110 Perez-Otano, I., Larsen, R. S. and Wesseling, J. F. (2016) Emerging roles of GluN3-containing
1111 NMDA receptors in the CNS. Nat Rev Neurosci **17**(10): 623-635.
1112 Pfeffer, C. K., Xue, M., He, M., Huang, Z. J. and Scanziani, M. (2013) Inhibition of inhibition in
1113 visual cortex: the logic of connections between molecularly distinct interneurons. Nat Neurosci
1114 **16**(8): 1068-1076.
1115 Picardo, M. A., Guigue, P., Bonifazi, P., Batista-Brito, R., Allene, C., Ribas, A., Fishell, G., Baude, A.
1116 and Cossart, R. (2011) Pioneer GABA cells comprise a subpopulation of hub neurons in the
1117 developing hippocampus. Neuron **71**(4): 695-709.
1118 Pina-Crespo, J. C., Talantova, M., Micu, I., States, B., Chen, H. S., Tu, S., Nakanishi, N., Tong, G.,
1119 Zhang, D., Heinemann, S. F., Zamponi, G. W., Stys, P. K. and Lipton, S. A. (2010) Excitatory glycine
1120 responses of CNS myelin mediated by NR1/NR3 "NMDA" receptor subunits. J Neurosci **30**(34):
1121 11501-11505.
1122 Pizzamiglio, L., Morice, E., Cardoso, C., Bossi, S., Mailhes-Hamon, C., Heimendahl, M. V.,
1123 Girardeau, G. and Paoletti, P. (2025) Excitatory glycine receptors control ventral hippocampus
1124 synaptic plasticity and anxiety-related behaviors. Proc Natl Acad Sci U S A **122**(37):
1125 e2501118122.
1126 Price, C. J., Cauli, B., Kovacs, E. R., Kulik, A., Lambolez, B., Shigemoto, R. and Capogna, M. (2005)
1127 Neurogliaform neurons form a novel inhibitory network in the hippocampal CA1 area. J
1128 Neurosci **25**(29): 6775-6786.
1129 Roberts, A. C., Diez-Garcia, J., Rodriguiz, R. M., Lopez, I. P., Lujan, R., Martinez-Turrillas, R., Pico,
1130 E., Henson, M. A., Bernardo, D. R., Jarrett, T. M., Clendeninn, D. J., Lopez-Mascaraque, L., Feng,
1131 G., Lo, D. C., Wesseling, J. F., Wetsel, W. C., Philpot, B. D. and Perez-Otano, I. (2009)
1132 Downregulation of NR3A-containing NMDARs is required for synapse maturation and memory
1133 consolidation. Neuron **63**(3): 342-356.
1134 Rouzbeh, N., Rau, A. R., Benton, A. J., Yi, F., Anderson, C. M., Johns, M. R., Jensen, L., Lotti, J. S.,
1135 Holley, D. C. and Hansen, K. B. (2023) Allosteric modulation of GluN1/GluN3 NMDA receptors by
1136 GluN1-selective competitive antagonists. J Gen Physiol **155**(6).
1137 Royer, S., Zemelman, B. V., Losonczy, A., Kim, J., Chance, F., Magee, J. C. and Buzsaki, G. (2012)
1138 Control of timing, rate and bursts of hippocampal place cells by dendritic and somatic inhibition.
1139 Nat Neurosci **15**(5): 769-775.
1140 Sanz, E., Yang, L., Su, T., Morris, D. R., McKnight, G. S. and Amieux, P. S. (2009) Cell-type-specific
1141 isolation of ribosome-associated mRNA from complex tissues. Proc Natl Acad Sci U S A **106**(33):
1142 13939-13944.
1143 Sasaki, Y. F., Rothe, T., Premkumar, L. S., Das, S., Cui, J., Talantova, M. V., Wong, H. K., Gong, X.,
1144 Chan, S. F., Zhang, D., Nakanishi, N., Sucher, N. J. and Lipton, S. A. (2002) Characterization and
1145 comparison of the NR3A subunit of the NMDA receptor in recombinant systems and primary
1146 cortical neurons. J Neurophysiol **87**(4): 2052-2063.
1147 Sik, A., Ylinen, A., Penttonen, M. and Buzsaki, G. (1994) Inhibitory CA1-CA3-hilar region feedback
1148 in the hippocampus. Science **265**(5179): 1722-1724.
1149 Siletti, K., Hodge, R., Mossi Albiach, A., Lee, K. W., Ding, S. L., Hu, L., Lonnerberg, P., Bakken, T.,
1150 Casper, T., Clark, M., Dee, N., Gloe, J., Hirschstein, D., Shapovalova, N. V., Keene, C. D., Nyhus, J.,

Tung, H., Yanny, A. M., Arenas, E., Lein, E. S. and Linnarsson, S. (2023) Transcriptomic diversity of cell types across the adult human brain. Science **382**(6667): eadd7046.
Somogyi, P., Katona, L., Klausberger, T., Lasztoczi, B. and Viney, T. J. (2014) Temporal redistribution of inhibition over neuronal subcellular domains underlies state-dependent rhythmic change of excitability in the hippocampus. Philos Trans R Soc Lond B Biol Sci **369**(1635): 20120518.
Stark, E., Roux, L., Eichler, R., Senzai, Y., Royer, S. and Buzsaki, G. (2014) Pyramidal cell-interneuron interactions underlie hippocampal ripple oscillations. Neuron **83**(2): 467-480.
Stuart, T., Butler, A., Hoffman, P., Hafemeister, C., Papalexi, E., Mauck, W. M., 3rd, Hao, Y., Stoeckius, M., Smibert, P. and Satija, R. (2019) Comprehensive Integration of Single-Cell Data. Cell **177**(7): 1888-1902 e1821.
Su, J., Basso, D., Iyer, S., Su, K., Wei, J. and Fox, M. A. (2020) Paracrine Role for Somatostatin Interneurons in the Assembly of Perisomatic Inhibitory Synapses. J Neurosci **40**(39): 7421-7435.
Sucher, N. J., Akbarian, S., Chi, C. L., Leclerc, C. L., Awobuluyi, M., Deitcher, D. L., Wu, M. K., Yuan, J. P., Jones, E. G. and Lipton, S. A. (1995) Developmental and regional expression pattern of a novel NMDA receptor-like subunit (NMDAR-L) in the rodent brain. J Neurosci **15**(10): 6509-6520.
Sun, L., Margolis, F. L., Shipley, M. T. and Lidow, M. S. (1998) Identification of a long variant of mRNA encoding the NR3 subunit of the NMDA receptor: its regional distribution and developmental expression in the rat brain. FEBS Lett **441**(3): 392-396.
Sunagawa, G. A., Sumiyama, K., Ukai-Tadenuma, M., Perrin, D., Fujishima, H., Ukai, H., Nishimura, O., Shi, S., Ohno, R. I., Narumi, R., Shimizu, Y., Tone, D., Ode, K. L., Kuraku, S. and Ueda, H. R. (2016) Mammalian Reverse Genetics without Crossing Reveals Nr3a as a Short-Sleeper Gene. Cell Rep **14**(3): 662-677.
Szabo, G. G., Farrell, J. S., Dudok, B., Hou, W. H., Ortiz, A. L., Varga, C., Moolchand, P., Gulsever, C. I., Gschwind, T., Dimidschstein, J., Capogna, M. and Soltesz, I. (2022) Ripple-selective GABAergic projection cells in the hippocampus. Neuron **110**(12): 1959-1977 e1959.
Taniguchi, H., He, M., Wu, P., Kim, S., Paik, R., Sugino, K., Kvitsiani, D., Fu, Y., Lu, J., Lin, Y., Miyoshi, G., Shima, Y., Fishell, G., Nelson, S. B. and Huang, Z. J. (2011) A resource of Cre driver lines for genetic targeting of GABAergic neurons in cerebral cortex. Neuron **71**(6): 995-1013.
Tasic, B. and Fishell, G. (2025) Exploring brain circuits, one cell type-or more- at a time. Neuron **113**(10): 1469-1473.
Tong, G., Takahashi, H., Tu, S., Shin, Y., Talantova, M., Zago, W., Xia, P., Nie, Z., Goetz, T., Zhang, D., Lipton, S. A. and Nakanishi, N. (2008) Modulation of NMDA receptor properties and synaptic transmission by the NR3A subunit in mouse hippocampal and cerebrocortical neurons. J Neurophysiol **99**(1): 122-132.
Tremblay, R., Lee, S. and Rudy, B. (2016) GABAergic Interneurons in the Neocortex: From Cellular Properties to Circuits. Neuron **91**(2): 260-292.
Tricoire, L., Pelkey, K. A., Daw, M. I., Sousa, V. H., Miyoshi, G., Jeffries, B., Cauli, B., Fishell, G. and McBain, C. J. (2010) Common origins of hippocampal Ivy and nitric oxide synthase expressing neurogliaform cells. J Neurosci **30**(6): 2165-2176.
Tricoire, L., Pelkey, K. A., Erkkila, B. E., Jeffries, B. W., Yuan, X. and McBain, C. J. (2011) A blueprint for the spatiotemporal origins of mouse hippocampal interneuron diversity. J Neurosci **31**(30): 10948-10970.

1195 Tsien, J. Z., Chen, D. F., Gerber, D., Tom, C., Mercer, E. H., Anderson, D. J., Mayford, M., Kandel, E.
1196 R. and Tonegawa, S. (1996) Subregion- and cell type-restricted gene knockout in mouse brain.
1197 Cell **87**(7): 1317-1326.
1198 Tuncdemir, S. N., Wamsley, B., Stam, F. J., Osakada, F., Goulding, M., Callaway, E. M., Rudy, B.
1199 and Fishell, G. (2016) Early Somatostatin Interneuron Connectivity Mediates the Maturation of
1200 Deep Layer Cortical Circuits. Neuron **89**(3): 521-535.
1201 Tzilivaki, A., Tukker, J. J., Maier, N., Poirazi, P., Sammons, R. P. and Schmitz, D. (2023)
1202 Hippocampal GABAergic interneurons and memory. Neuron **111**(20): 3154-3175.
1203 Varga, C., Golshani, P. and Soltesz, I. (2012) Frequency-invariant temporal ordering of
1204 interneuronal discharges during hippocampal oscillations in awake mice. Proc Natl Acad Sci U S
1205 A **109**(40): E2726-2734.
1206 Vong, L., Ye, C., Yang, Z., Choi, B., Chua, S., Jr. and Lowell, B. B. (2011) Leptin action on
1207 GABAergic neurons prevents obesity and reduces inhibitory tone to POMC neurons. Neuron
1208 **71**(1): 142-154.
1209 Wang, C. Z., Ma, J., Xu, Y. Q., Jiang, S. N., Chen, T. Q., Yuan, Z. L., Mao, X. Y., Zhang, S. Q., Liu, L. Y.,
1210 Fu, Y. and Yu, Y. C. (2019) Early-generated interneurons regulate neuronal circuit formation
1211 during early postnatal development. Elife **8**.
1212 Wee, K. S., Tan, F. C., Cheong, Y. P., Khanna, S. and Low, C. M. (2016) Ontogenic Profile and
1213 Synaptic Distribution of GluN3 Proteins in the Rat Brain and Hippocampal Neurons. Neurochem
1214 Res **41**(1-2): 290-297.
1215 Wester, J. C. and McBain, C. J. (2016) Interneurons Differentially Contribute to Spontaneous
1216 Network Activity in the Developing Hippocampus Dependent on Their Embryonic Lineage. J
1217 Neurosci **36**(9): 2646-2662.
1218 Wong, H. K., Liu, X. B., Matos, M. F., Chan, S. F., Perez-Otano, I., Boysen, M., Cui, J., Nakanishi, N.,
1219 Trimmer, J. S., Jones, E. G., Lipton, S. A. and Sucher, N. J. (2002) Temporal and regional
1220 expression of NMDA receptor subunit NR3A in the mammalian brain. J Comp Neurol **450**(4):
1221 303-317.
1222 Xu, Q., Tam, M. and Anderson, S. A. (2008) Fate mapping Nkx2.1-lineage cells in the mouse
1223 telencephalon. J Comp Neurol **506**(1): 16-29.
1224 Yang, J., Wang, S., Yang, Z., Hodgkinson, C. A., Iarikova, P., Ma, J. Z., Payne, T. J., Goldman, D. and
1225 Li, M. D. (2015) The contribution of rare and common variants in 30 genes to risk nicotine
1226 dependence. Mol Psychiatry **20**(11): 1467-1478.
1227 Yao, Y. and Mayer, M. L. (2006) Characterization of a soluble ligand binding domain of the NMDA
1228 receptor regulatory subunit NR3A. J Neurosci **26**(17): 4559-4566.
1229 Yao, Z., van Velthoven, C. T. J., Nguyen, T. N., Goldy, J., Sedeno-Cortes, A. E., Baftizadeh, F.,
1230 Bertagnolli, D., Casper, T., Chiang, M., Crichton, K., Ding, S. L., Fong, O., Garren, E., Glandon, A.,
1231 Gouwens, N. W., Gray, J., Graybuck, L. T., Hawrylycz, M. J., Hirschstein, D., Kroll, M., Lathia, K.,
1232 Lee, C., Levi, B., McMillen, D., Mok, S., Pham, T., Ren, Q., Rimorin, C., Shapovalova, N., Sulc, J.,
1233 Sunkin, S. M., Tieu, M., Torkelson, A., Tung, H., Ward, K., Dee, N., Smith, K. A., Tasic, B. and Zeng,
1234 H. (2021) A taxonomy of transcriptomic cell types across the isocortex and hippocampal
1235 formation. Cell **184**(12): 3222-3241 e3226.
1236 Yao, Z., van Velthoven, C. T. J., Kunst, M., Zhang, M., McMillen, D., Lee, C., Jung, W., Goldy, J.,
1237 Abdelhak, A., Aitken, M., Baker, K., Baker, P., Barkan, E., Bertagnolli, D., Bhandiwad, A., Bielstein,
1238 C., Bishwakarma, P., Campos, J., Carey, D., Casper, T., Chakka, A. B., Chakrabarty, R., Chavan, S.,

Chen, M., Clark, M., Close, J., Crichton, K., Daniel, S., DiValentin, P., Dolbeare, T., Ellingwood, L., Fiabane, E., Fliss, T., Gee, J., Gerstenberger, J., Glandon, A., Gloe, J., Gould, J., Gray, J., Guilford, N., Guzman, J., Hirschstein, D., Ho, W., Hooper, M., Huang, M., Hupp, M., Jin, K., Kroll, M., Lathia, K., Leon, A., Li, S., Long, B., Madigan, Z., Malloy, J., Malone, J., Maltzer, Z., Martin, N., McCue, R., McGinty, R., Mei, N., Melchor, J., Meyerdierks, E., Mollenkopf, T., Moonsman, S., Nguyen, T. N., Otto, S., Pham, T., Rimorin, C., Ruiz, A., Sanchez, R., Sawyer, L., Shapovalova, N., Shepard, N., Slaughterbeck, C., Sulc, J., Tieu, M., Torkelson, A., Tung, H., Valera Cuevas, N., Vance, S., Wadhwani, K., Ward, K., Levi, B., Farrell, C., Young, R., Staats, B., Wang, M. M., Thompson, C. L., Mufti, S., Pagan, C. M., Kruse, L., Dee, N., Sunkin, S. M., Esposito, L., Hawrylycz, M. J., Waters, J., Ng, L., Smith, K., Tasic, B., Zhuang, X. and Zeng, H. (2023) A high-resolution transcriptomic and spatial atlas of cell types in the whole mouse brain. Nature **624**(7991): 317-332.

Yuan, T., Mameli, M., O'Connor, E. C., Dey, P. N., Verpelli, C., Sala, C., Perez-Otano, I., Luscher, C. and Bellone, C. (2013) Expression of cocaine-evoked synaptic plasticity by GluN3A-containing NMDA receptors. Neuron **80**(4): 1025-1038.

Zeilhofer, H. U., Studler, B., Arabadzisz, D., Schweizer, C., Ahmadi, S., Layh, B., Bosl, M. R. and Fritschy, J. M. (2005) Glycinergic neurons expressing enhanced green fluorescent protein in bacterial artificial chromosome transgenic mice. J Comp Neurol **482**(2): 123-141.

Zeisel, A., Munoz-Manchado, A. B., Codeluppi, S., Lonnerberg, P., La Manno, G., Jureus, A., Marques, S., Munguba, H., He, L., Betsholtz, C., Rolny, C., Castelo-Branco, G., Hjerling-Leffler, J. and Linnarsson, S. (2015) Brain structure. Cell types in the mouse cortex and hippocampus revealed by single-cell RNA-seq. Science **347**(6226): 1138-1142.

Zhang, X. Y., Liu, A. P., Ruan, D. Y. and Liu, J. (2002) Effect of developmental lead exposure on the expression of specific NMDA receptor subunit mRNAs in the hippocampus of neonatal rats by digoxigenin-labeled in situ hybridization histochemistry. Neurotoxicol Teratol **24**(2): 149-160.

Zhu, Z., Yi, F., Epplin, M. P., Liu, D., Summer, S. L., Mizu, R., Shaulsky, G., XiangWei, W., Tang, W., Burger, P. B., Menaldino, D. S., Myers, S. J., Liotta, D. C., Hansen, K. B., Yuan, H. and Traynelis, S. F. (2020) Negative allosteric modulation of GluN1/GluN3 NMDA receptors. Neuropharmacology **176**: 108117.

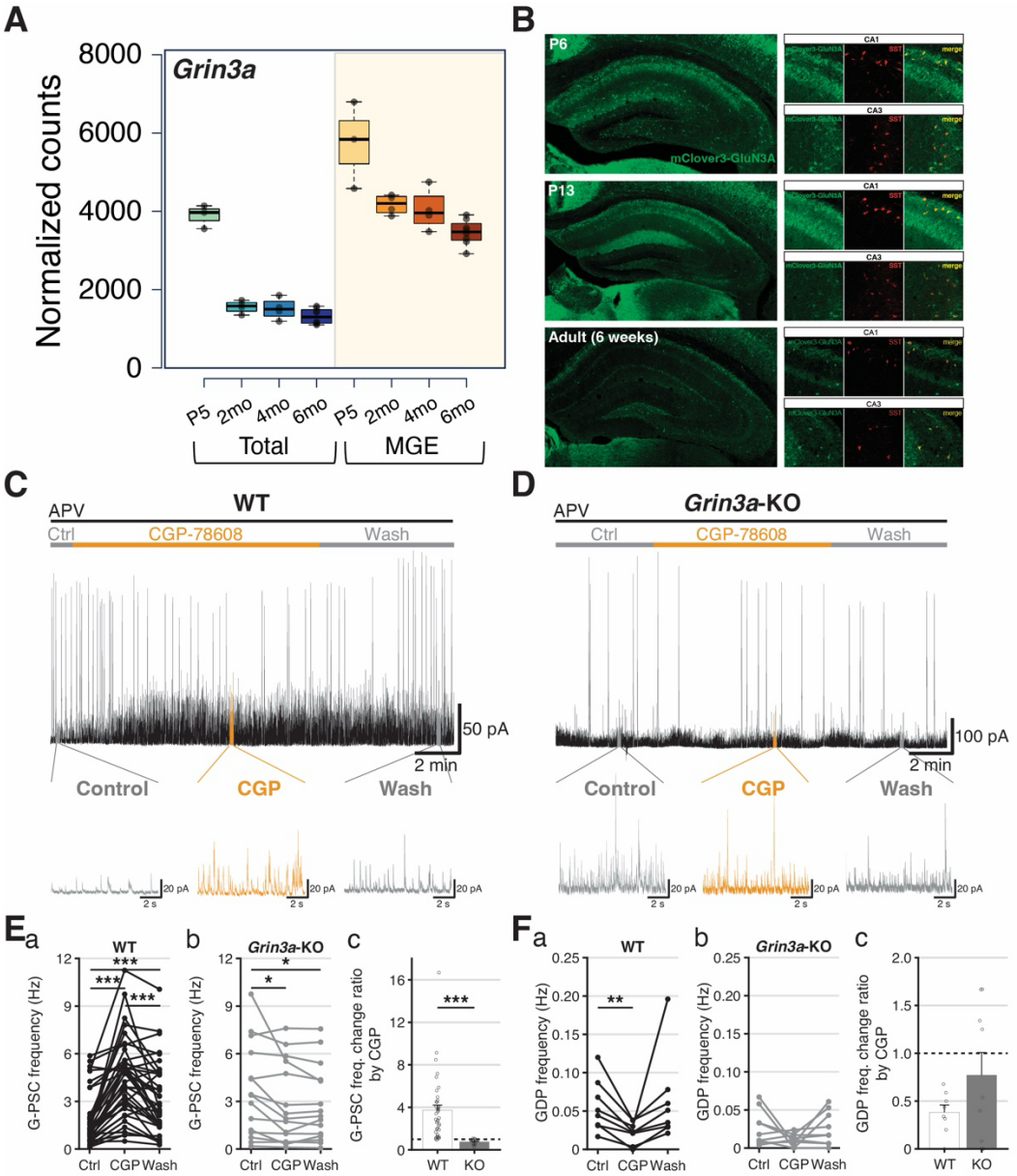

Figure 1. Developmental expression of *Grin3a* transcripts and G-PSC/GDP modulation by functional eGlyRs in early postnatal hippocampus. A. Developmental profile of *Grin3a* single RNA-seq data hippocampus using Ribo-tag. **B.** Developmental change of GluN3a expression images from mClover3-GluN1a mice demonstrating significant co-expression with somatostatin (Sst). **C-D.** Single trace example of spontaneous GABAergic postsynaptic currents (G-PSCs) and GDPs in CA3 pyramidal neurons (PNs) from WT (C), *Grin3a*-KO mouse brain slices (D). **E.** G-PSC frequency change in (a) WT, (b) *Grin3a*-KO, and (c) comparison of G-PSC frequency change ratio by CGP. **F.** Giant depolarizing potential (GDP) frequency change in WT (a), *Grin3a*-KO (b), and normalized comparison of GDP frequency change by CGP in WT and *Grin3a*-KO mice (c). (WT: 62 cells/slices from 26 mice, P4.5-8.5), *Grin3a*-KO: 32 cells/slices from 13 mice, P5.5-12.5 *pre-incubated in APV 100 µM.

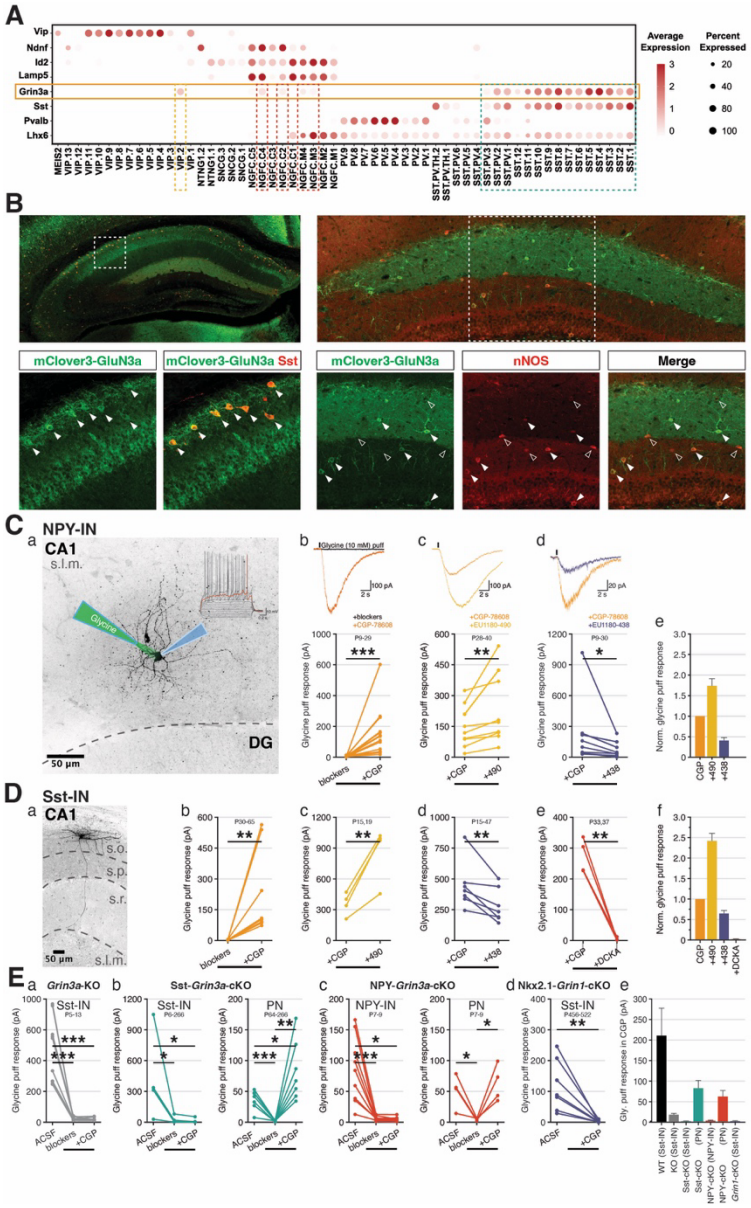

Figure 2. *Grin3a* expression and functional eGlyR-mediated currents in adult hippocampal INs. **A.** Survey of *Grin3a* expression across major GABAergic interneuron classes (Sst, somatostatin-expressing cells; PV, Parvalbumin-expressing cells; NGFC, neurogliaform cells; VIP, vaso-intestinal peptide-expressing cells) from mice cortex and hippocampus. **B.** Co-expression of *Grin3a* with Sst (left), and nNOS (right) respectively. **C.**(a) Whole cell patch-clamping an NPY-IN with glycine puff. Glycine puff response of NPY-IN in (b) desensitization reducer (CGP), (c) allosteric modulators positive (490), (d) negative (438), and (e) normalized glycine puff responses. **D.**(a) A sample image of Sst-IN (OLM-IN) (b) Glycine puff response of Sst-IN in CGP, (c-d) allosteric positive/negative modulators, respectively, (e) competitive eGlyR blocker (DCKA), and (f) normalized glycine puff responses. **E.** Glycine puff responses of (a) Sst-IN in *Grin3a*-KO mice, (b) Sst-IN and PN in Sst-*Grin3a*-cKO, (c) NPY-IN and PN in NPY-*Grin3a*-cKO, and (d) Sst-IN in Nkx2.1-*Grin1*-cKO, and (e) average glycine puff responses.

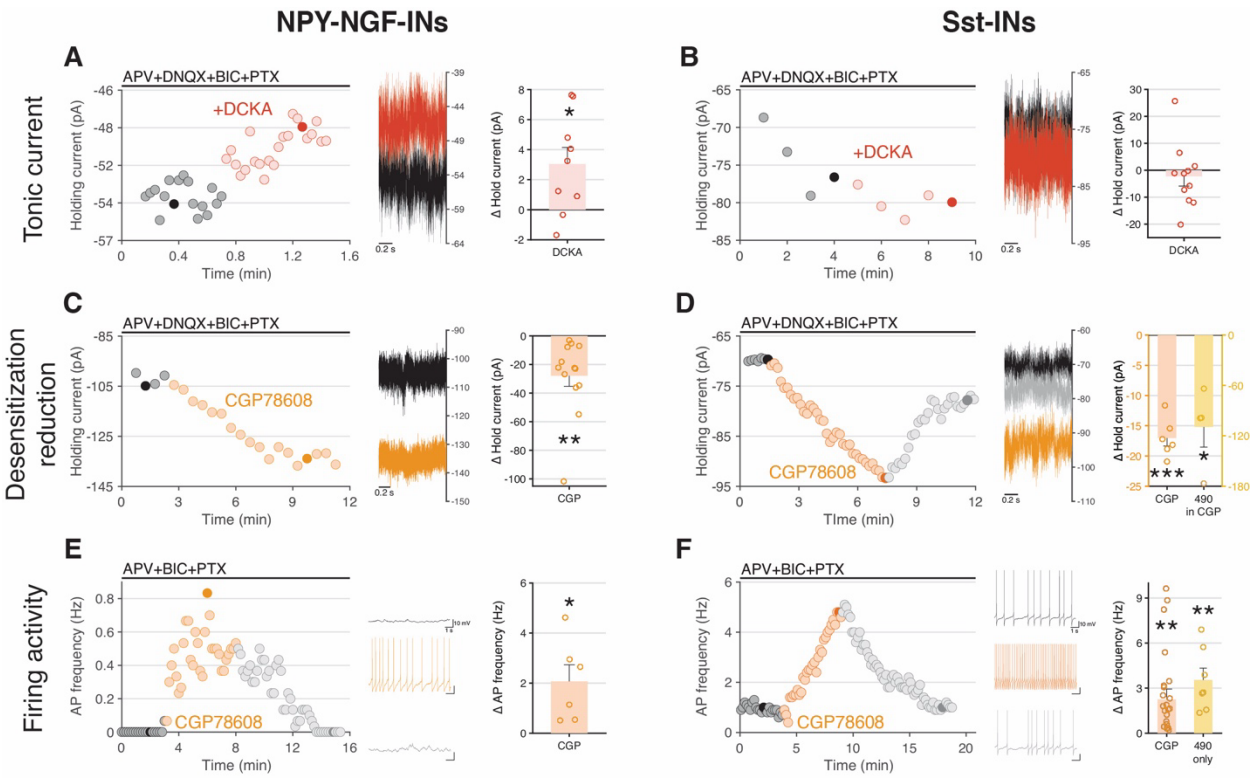

Figure 3. eGlyRs are tonically liganded by endogenous glycine in hippocampal SST and NPY-NGF-INs. A-B. eGlyR tonic current blocked by DCKA in NPY-INs, but no tonic current in Sst-INs. **C-D.** Holding current increase by desensitization reduction by CGP and/or EU1180-490 in NPY-INs and Sst-IN respectively. **E-F.** Firing activity increase by CGP or EU1180-490 in NPY-INs and Sst-INs respectively.

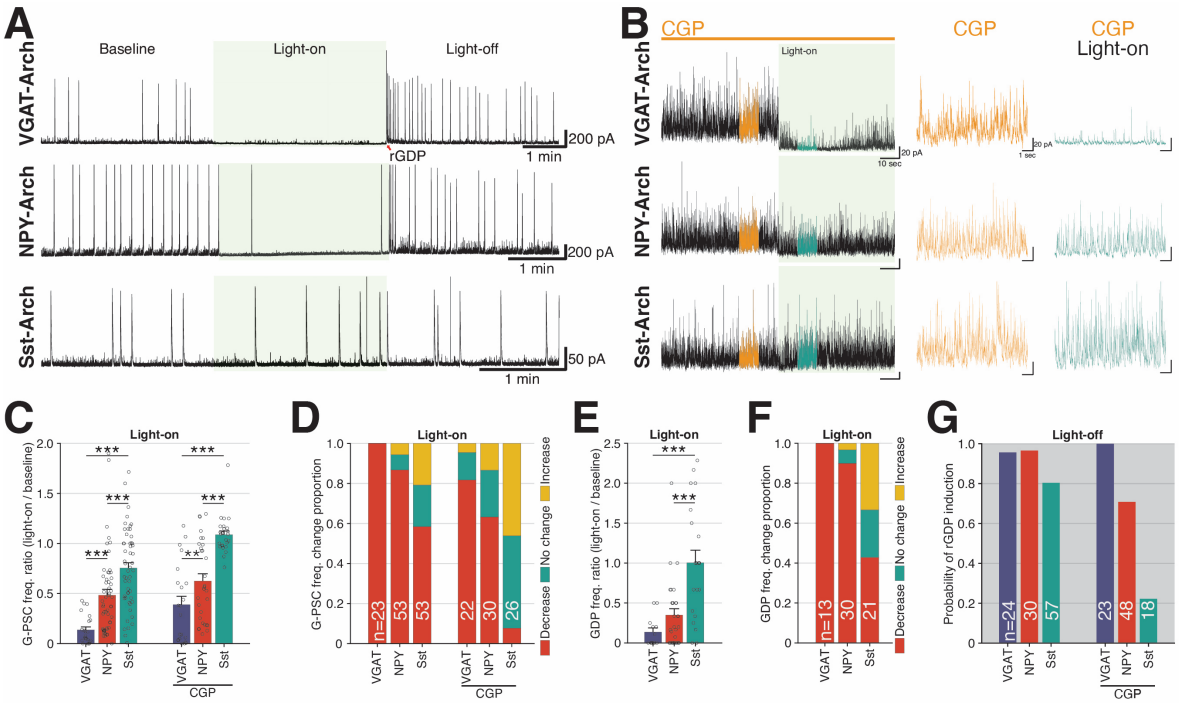

Figure 4. Relative contributions of NPY-NGF and SST INs in eliciting early hippocampal inhibition and network synchrony. A. Whole-cell recording samples of CA3-PN in brain slices from VGAT-ArCh (top), NPY-ArCh (middle), and Sst-ArCh (bottom) mice with light-stimulation. **B.** Examples of G-PSC change by light-on in presence of CGP-78608 in CA3-PN in hippocampal slices from VGAT-ArCh (top), NPY-ArCh (middle), and Sst-ArCh (bottom) mice **C.** G-PSC frequency change ratio by light-on in VGAT-Arch, NPY-Arch, and Sst-Arch mouse hippocampus. **D.** G-PSC frequency change proportion; decrease (red), change less than +- 10 % (green), and increase (yellow). **E.** GDP frequency change ratio by light-on. **F.** Light-on evoked GDP frequency change proportion; decrease (red), no change (green), increase (yellow). **G.** Probability of light-off-evoked rebound GDP (rGDP). (VGAT-Arch: 20 cells/slices from 5 mice, P6.5-8.5, NPY-Arch: 39 cells/slices from 10 mice, P5.5-8.5, Sst-Arch: 30 cells/slices from 10 mice, P5.5-8.5).

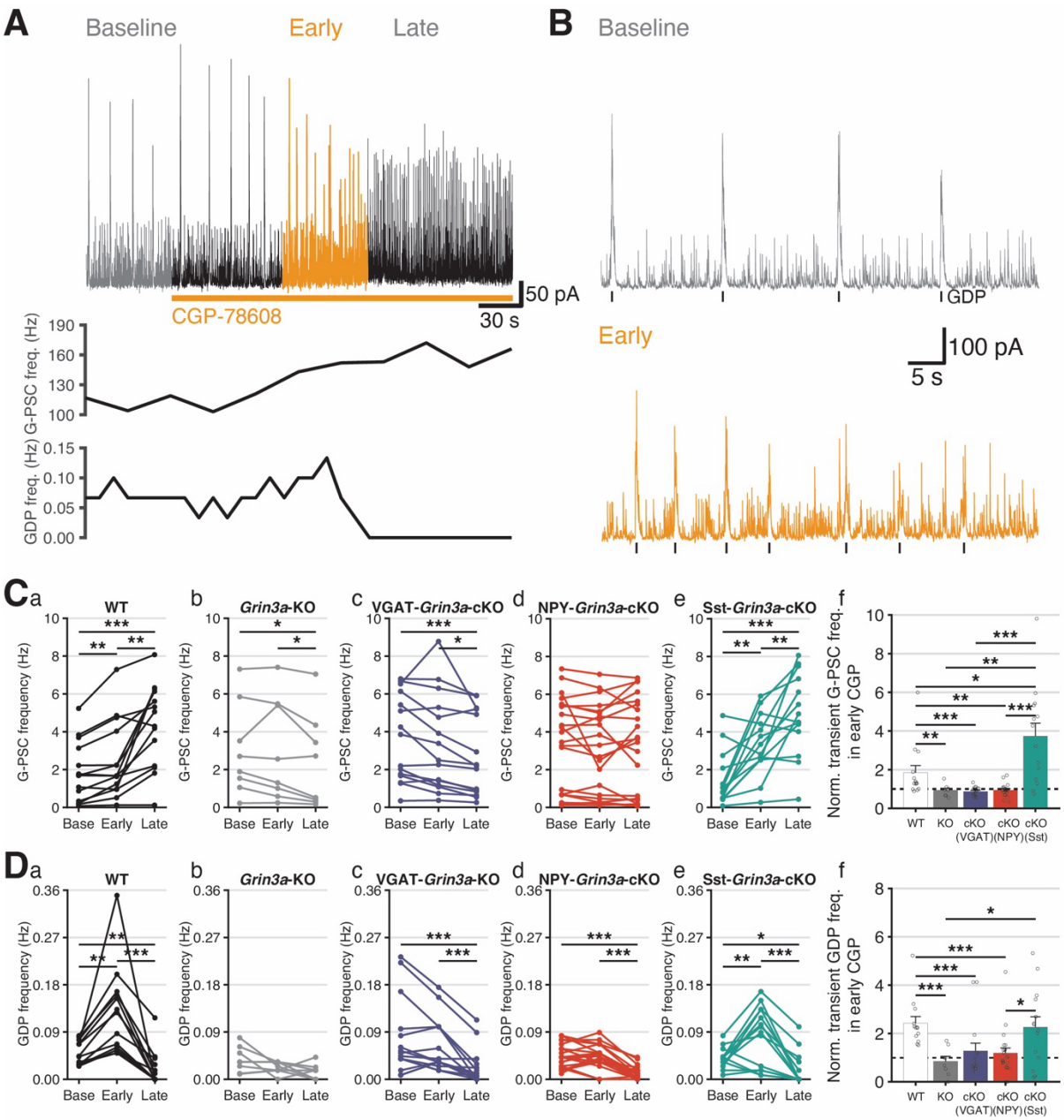

Figure 5. Recruitment of GABAergic tone and GDP generation is predominantly mediated by activation of eGlyRs expressed on NPY-NGF-INs. A. An example recording of GDP with CGP-78608 (upper), G-PSC frequency (middle), and GDP frequency (bottom). **B.** Enlarged traces in baseline (upper)/CGP-Early(bottom) phases from A. **C.** G-PSC frequency change before, immediate (early) and stable (late) phase of CGP application in (a) WT, (b) *Grin3a*-KO, (c) VGAT-*Grin3a*-cKO, (d) NPY-*Grin3a*-cKO, (e) Sst-*Grin3a*-cKO mouse hippocampal slices, and (f) normalized immediate G-PSC frequency change by CGP. **D.** GDP frequency change before, early and late CGP application in (a) WT, (b) *Grin3a*-KO, (c) VGAT-*Grin3a*-cKO, (d) NPY-*Grin3a*-cKO, (e) Sst-*Grin3a*-cKO mouse hippocampal slices, and (f) normalized immediate GDP frequency change by CGP.

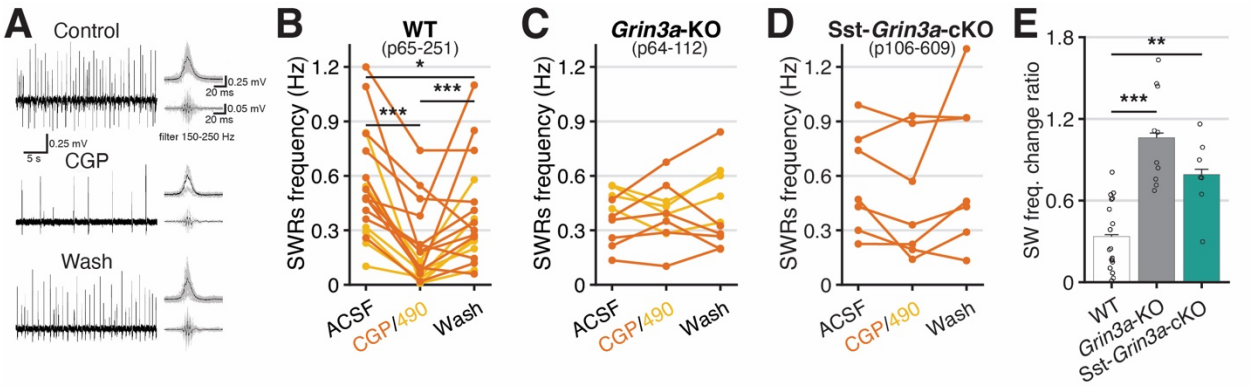

Figure 6. Activation of eGlyRs shape adult hippocampal sharp wave ripple dynamics. A. An example of sharp wave ripples. **B-D.** Sharp wave frequency change by CGP-78608/EU1180-490 in WT, *Grin3a*-KO, and Sst-*Grin3a*-cKO, respectively. **E.** SPW change rate in drug normalized by frequency in ACSF. All recordings were performed with APV (50 µM) in bath solution.

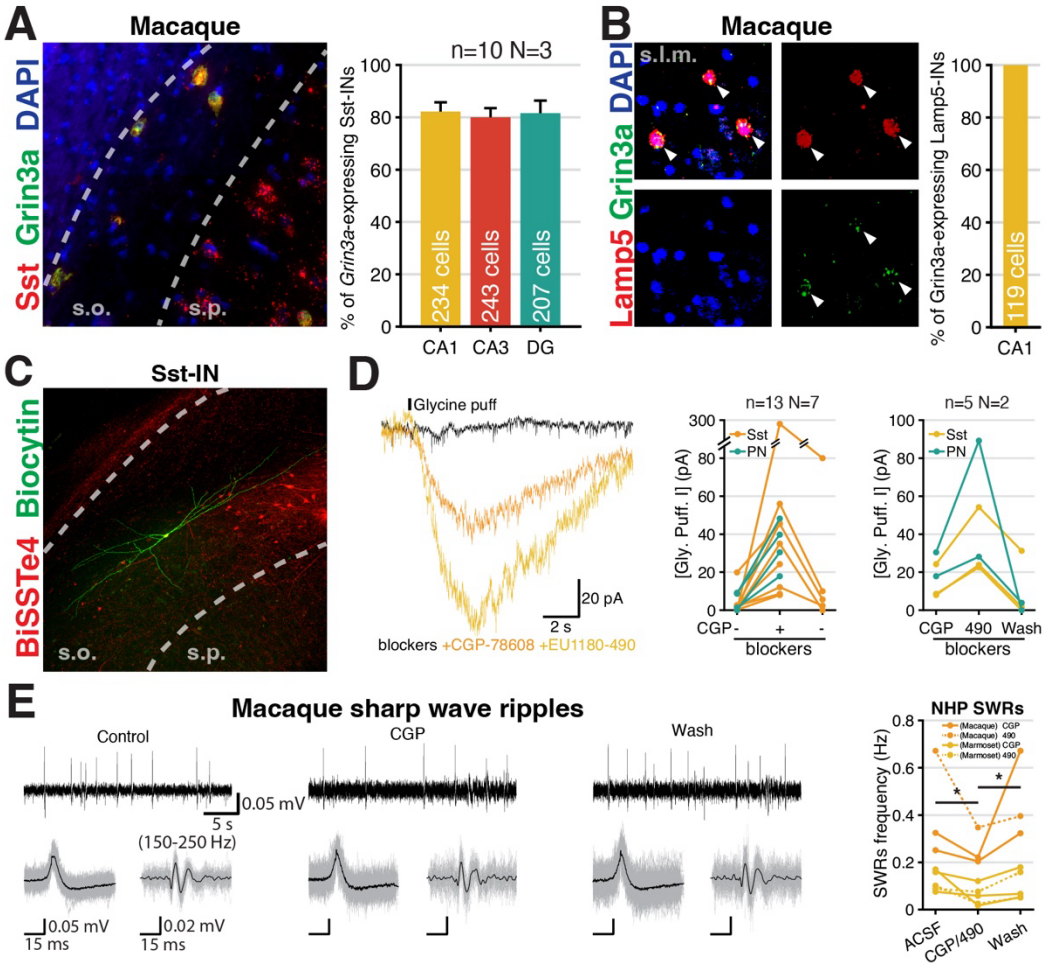

Figure 7. Evolutionary conservation of hippocampal interneuron eGlyR functional expression and role in network rhythmogenesis. A. Co-expression of Sst and *Grin3a* in a Macaque CA3 (stratum oriens) slice. **B.** Co-expression of Lamp5 and *Grin3a*. **C.** An example image of Sst-IN reported by pAAV-PHP.eB-BiSSTe4-dTomato (red) and post-hoc cell morphology recovery (green) in Macaque CA1 hippocampus. **D.** Glycine puff response of Sst-INs and PNs with CGP-78608 (middle) and CGP-78608 + EU1180-490 (right) in macaque hippocampus. **E.** SWRs frequency change by CGP-78608 / EU1180-490 in macaque (n=3, N=2) and marmoset (n=5, N=2). (n: number of slices, N: number of animals)

1339 **S1**

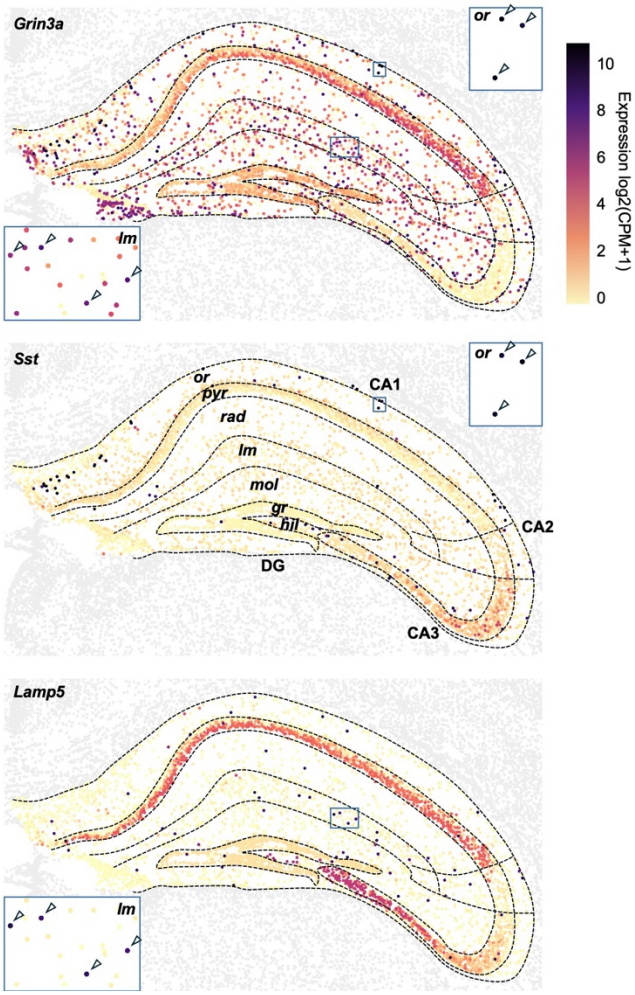

1340
1341 ***Grin3a* is absent in CA3 PNs and enriched in *Sst* and *Lamp5* expressing cells.** Publicly available
1342 spatial transcriptomics MERFISH data from the Allen Brain Cell Atlas with imputed gene
1343 expression [Yao2023]. Visualized gene expression restricted to the hippocampal formation,
1344 showing (top) *Grin3a*, (middle) *Sst*, and (bottom) *Lamp5*. Insets highlight expression of putative
1345 Sst-INs in stratum oriens (or) and Lamp5-INs in stratum lacunosum-moleculare (lm). Arrows
1346 denote significant expression of Grin3A transcript in SST or Lamp5 expressing INs.

1347 **S2**

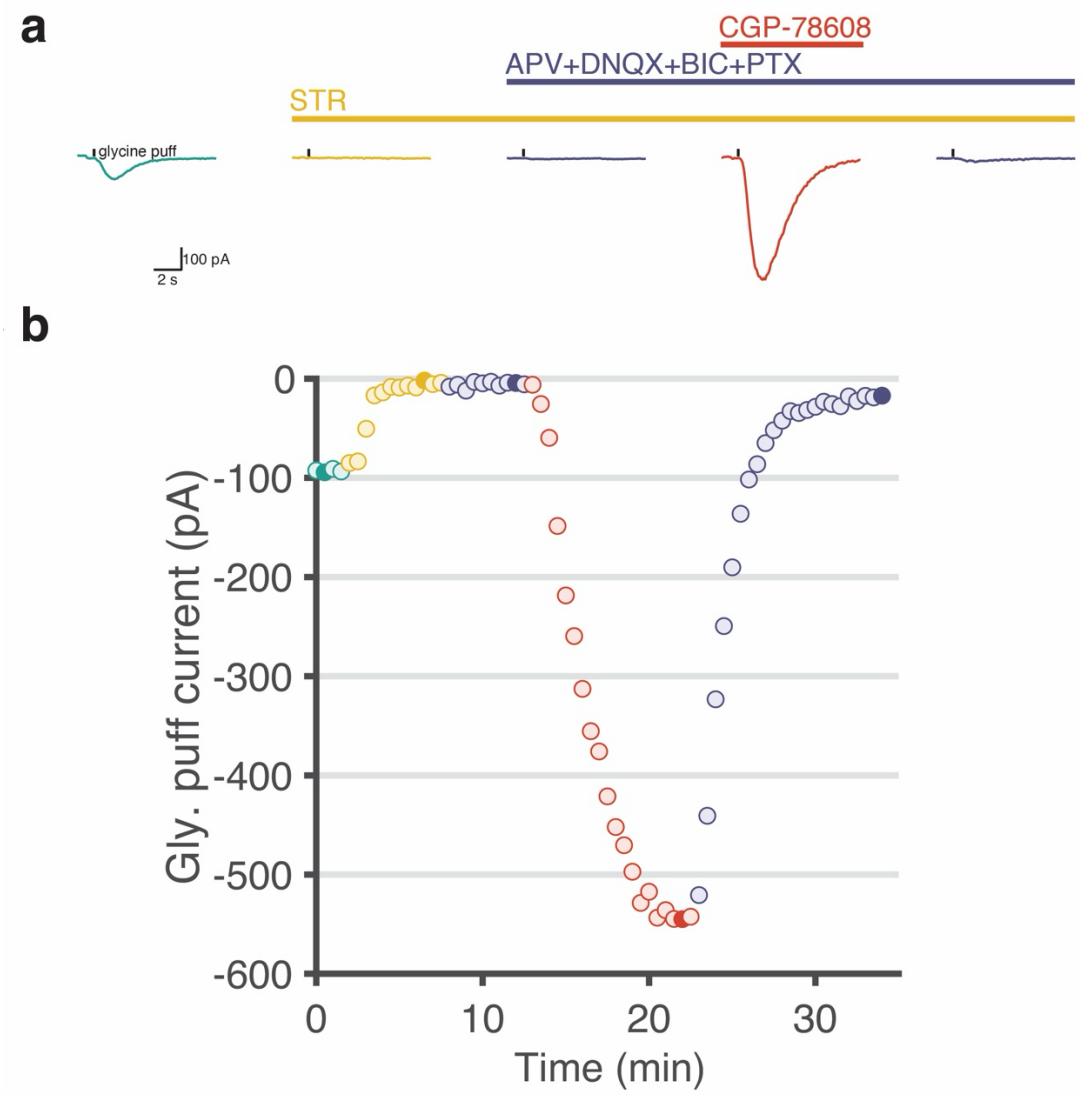

1348
1349 **Experimental procedure employed to isolate strychnine-insensitive glycine evoked eGlyR**
1350 **mediated depolarizing currents.** (a) Example current traces from a CA1 Sst-IN with glycine puff
1351 responses in presence of blockers and CGP-78608, filled circles in (b). Strychnine sensitive
1352 eGlyR-mediated current prominently contributed the glycine response current in ACSF. (b)
1353 Glycine puff currents in antagonists and CGP-78608. * STR 1 μM, APV 50 μM, DNQX 10 μM, BIC
1354 10 uM and PTX 50 μM.

1355 **S3**

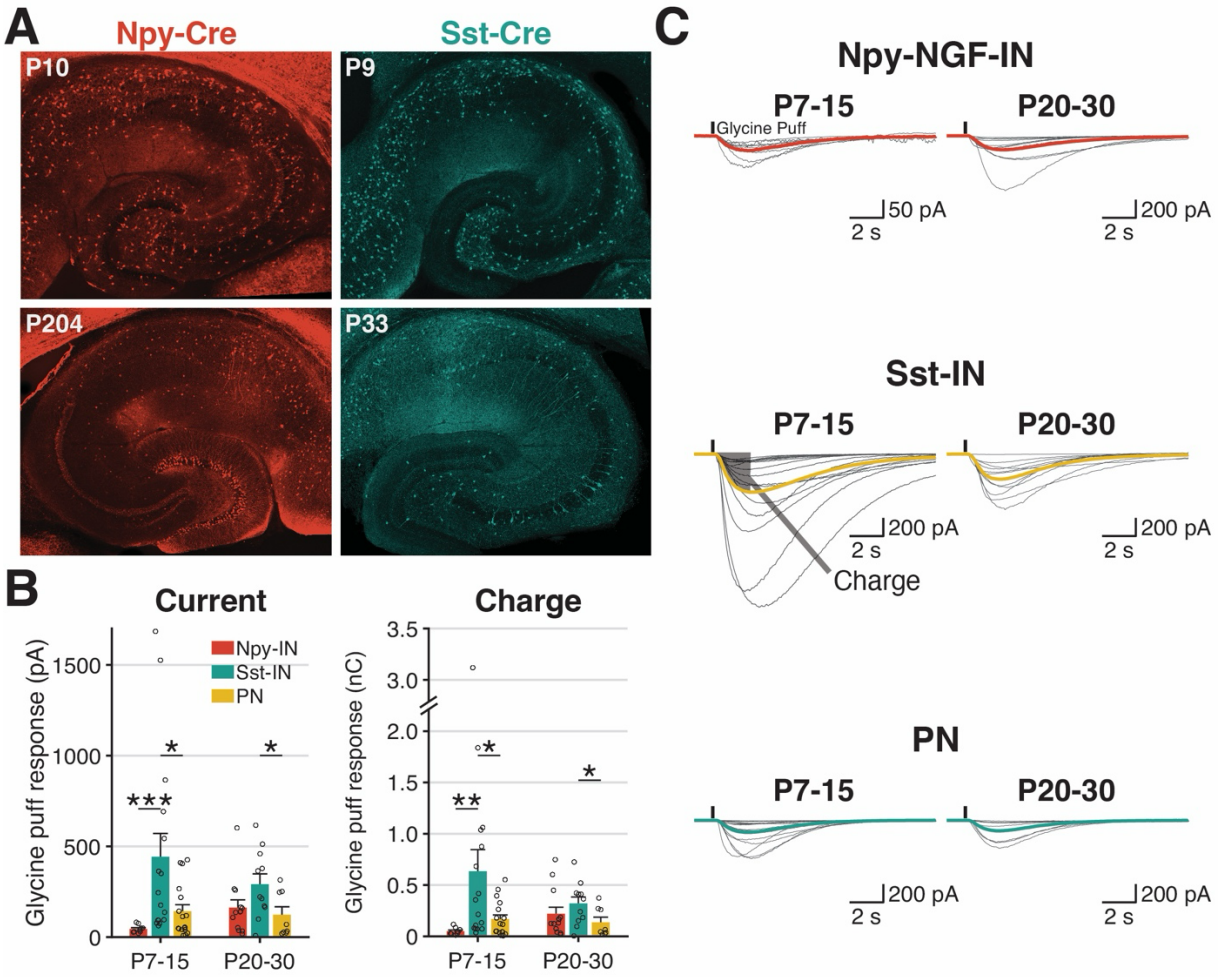

1356

1357 **eGlyRs mediate functional responses in SST and NPY-NGFC INs throughout development. A.**
1358 Sample images of postnatal (top)/adulthood (bottom), NPY-IRES-Cre (left)/Sst-IRES-Cre (right)
1359 mouse hippocampal slices. **B.** (left) Glycine puff response currents in NPY-INs, Sst-INs, and PNs
1360 from postnatal and adulthood mice. (right) Glycine puff response charge transfer in NPY-INs, Sst-
1361 INs, and PNs from postnatal and adulthood mice. **C.** Glycine puff responses in NPY -INs, Sst-INs
1362 and PNs in different ages. Thick lines are average puff responses of cells and gray lines are
1363 average puff responses of trials in each cell.

1364

1365 **S4**

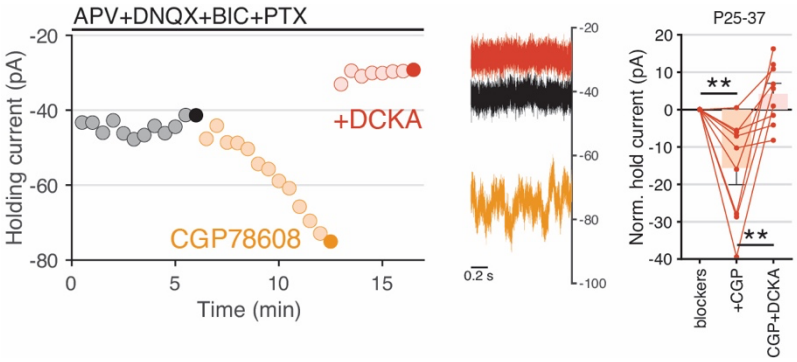

1366

1367 **DCKA sensitivity of CGP78608-induced change holding current in hippocampal interneurons.**
1368 Shown are the time course (left) and traces (middle) from a representative sample NGFC
1369 recording illustrating increased holding current (V_h=-70mV) in response to CGP78608 and
1370 subsequent reduction of holding current upon DCKA application. At right, is the group data
1371 summarizing the effects of CGP and subsequent DCKA application upon holding currents for Sst-
1372 INs and NGFCs combined.

1373 **S5**

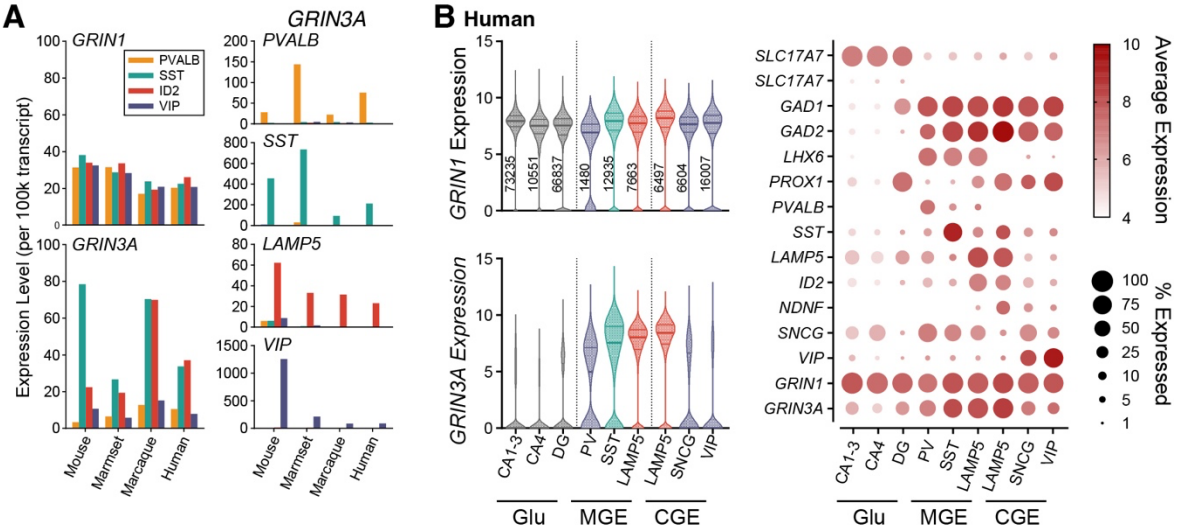

1374

1375 ***GRIN1* and *GRIN3A* expression cross species. A.** Publicly-available snRNA-seq mean expression
1376 in neocortical IN subpopulations PVALB (orange), SST (cyan), ID2/LAMP5 (red) and VIP (purple)
1377 across mouse, marmoset, macaque, and human [Krienen2020], for (left) *GRIN1* and *GRIN3A* and
1378 (right) distinguishing markers *PVALB*, *SST*, *LAMP5*, and *VIP*. **B.** Publicly-available snRNA-seq of
1379 human hippocampal neurons [Siletti2023], with (left) *GRIN1* and *GRIN3A* expression in
1380 glutamatergic (Glu) superclusters and grouped MGE and CGE clusters (see Methods), and (right)
1381 dot plot of distinguishing marker genes and *GRIN1*, *GRIN3A*.

1382